**Review Article** **Open Access**

Feng Li, Jinhui Yuan*, Zhe Kang, Qian Li, and P. K. A. Wai

# Modeling Frequency Comb Sources

DOI 10.1515/nanoph-2016-0030
Received September 30, 2015; accepted February 23, 2016

**Abstract:** Frequency comb sources have revolutionized metrology and spectroscopy and found applications in many fields. Stable, low-cost, high-quality frequency comb sources are important to these applications. Modeling of the frequency comb sources will help the understanding of the operation mechanism and optimization of the design of such sources. In this paper, we review the theoretical models used and recent progress of the modeling of frequency comb sources.

**Keywords:** Optical frequency comb; modeling; mode-locked laser; supercontinuum generation; Kerr comb

## 1 Introduction

Ever since the invention of lasers, advances in photonics have brought significant breakthroughs in many branches of science and engineering. The latest example is the generation of frequency comb sources which finds applications in metrology, optical atomic clocks, high precision spectroscopy, etc [1–5]. Optical frequency comb generation was cited in the 2005 Nobel Prize in Physics. Stable, low-cost and high-quality frequency comb sources are expected to bring in revolutionary changes in others fields such as high-speed optical data transmission and ultrafast signal processing.

Recently, modeling has become an integral part of research in photonics. Cumulative efforts in the theory and modeling of the performance of photonic devices in the past decades have resulted in many theoretical models, the predictions of which match the experimental observations well. Availability of commercial numerical packages encapsulating these models allows easy access of powerful simulation tools to many. Simulation results are now routinely used to "explain" experimental observations and guide the design of experiments. However, it is important to remember that a model is only as good as our "understanding" of the physical mechanisms of the phenomenon or application being studied. The choice of the physical effects to be included in a model is the key to the success in theory and modeling, but it can also be easily misused. Thus results from modeling and simulation should always be handled with care. It is important to bear in mind that qualitative similarity between experimental observations and simulation results are only supporting evidence of the validity of the model, it is certainly not a proof.

The key technology in frequency comb generation is the method to stabilize the carrier-envelope phase (CEP) of an optical pulse train [1, 2, 6, 7]. Figure 1A shows that if the laser spectrum spans an octave or more, the laser cavity can be fully stabilized by using self-referencing CEP methods based on the *f*-2*f* detection technique with second harmonic generation (SHG) [1]. The second harmonic of the one of the frequency comb teeth at lower frequency $f_l$ is identical to a high-frequency component $f_h$ except for a possible phase mismatch $\delta$, which is related to the carrier envelope offset frequency $f_{ceo}$. The phase mismatch $\delta$ can be eliminated by using feedback control on the beating signal between the frequency components $2f_l$ and $f_h$. The resulting spectrum of the mode-locked laser will then be fully stabilized. If octave spanning spectra are not available, high-order harmonics technique, such as 2*f*-3*f* self-referencing, which uses SHG and third harmonic generation (THG) to generate two slightly mismatched frequencies, can also be applied [8–10] as shown in Figure 1B. If self-referencing stabilization is not possible, then the laser can be stabilized by locking to other stable light sources via a frequency chain as shown in Figure 1C, which was widely used in frequency chain techniques from many years ago [11, 12]. Since the self-referencing mechanism to stabilize the CEP is rather mature, especially when octave spanning spectra are available, it will not be the focus of this review. Interested readers can refer to Refs. [13–16] and the references therein. As we devote this review to

**Feng Li, Zhe Kang, P. K. A. Wai:** Photonics Research Centre, Department of Electronic and Information Engineering, The Hong Kong Polytechnic University, Hong Kong SAR, P. R. China
***Corresponding Author: Jinhui Yuan:** Photonics Research Centre, Department of Electronic and Information Engineering, The Hong Kong Polytechnic University, Hong Kong SAR, P. R. China; and State Key Laboratory of Information Photonics and Optical Communications, Beijing University of Posts and Telecommunications, Beijing 100876, China; E-mail: yuanjinhui81@163.com
**Qian Li:** School of Electronic and Computer Engineering, Peking University, Shenzhen, 518055, China

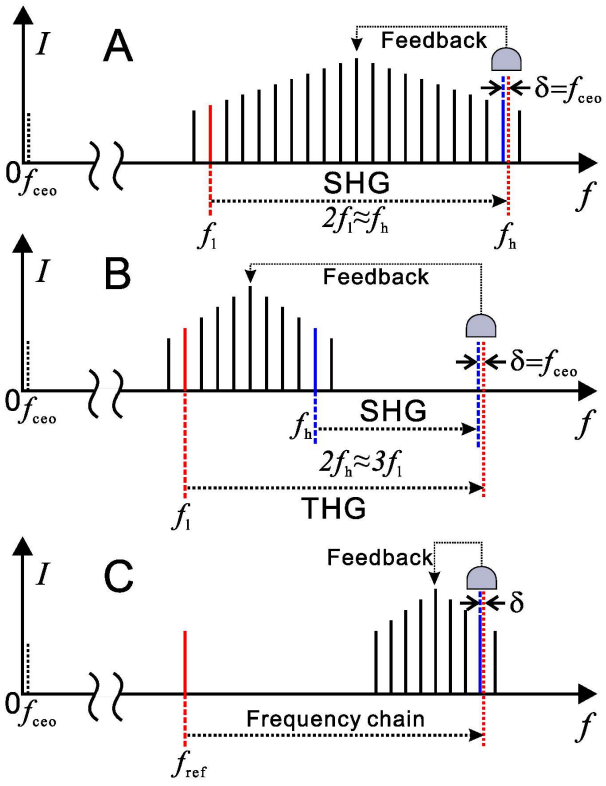


**Figure 1:** Self-referencing carrier envelope phase stabilization with (A) $f$-$2f$ and (B) $2f$-$3f$ mismatch detection techniques and (C) external referencing carrier envelope phase stabilization to lock the comb spectrum to a known frequency $f_{ref}$ via the bridging of a frequency chain.

the modeling of the generation of octave spanning optical sources only, we assume that some feedback mechanisms have been utilized to stabilize the CEP. We also assume that the self-referencing CEP control mechanism does not affect the generation of the octave spanning optical output except to stabilize its CEP. We note that in most theoretical models describing the evolution of optical pulses in dielectric media or photonic devices, the rapid oscillation at the optical carrier frequency is removed by using the slowly varying envelope approximation. Only the evolution of the envelope of the electric field is studied. Most of the models reviewed in this paper will fall into this category.

Highly stabilized mode-locked lasers are by far the most popular optical frequency comb sources [15–17]. However, generation of octave spanning spectra, or equivalently few femtosecond pulses, directly from a mode-locked laser remains a challenging task. It is a feat that has been demonstrated by solid state lasers only [18] and is still beyond the reach of fiber lasers [19]. Instead of direct generation from a mode-locked laser, octave spanning spectra can also be obtained by expanding the spectra of a mode-locked laser output in a highly nonlinear medium such as a photonic crystal fiber (PCF), in a process known as supercontinuum (SC) generation [20]. The most desirable features of using mode-locked lasers to generate coherent octave spanning supercontinua are the high peak power and ultrashort duration of the laser pulses. Typically, pulse duration less than 100 fs and peak power of several kilowatts are the minimum requirements for the pulses to ensure the coherence of the generated supercontinuum [20]. Kerr combs, discovered in 2007 [21], are another significant class of optical frequency comb sources. The frequency comb is generated by coupling a single continuous wave pump source into a high-finesse microresonator [21]. The CW pump source interacts with the modes of the microresonator by Kerr nonlinearity, and forms the hyperparametric oscillation [22–24] i.e., the combination of modulation instability (MI) and cascaded four-wave-mixing (FWM).

In the following, we review recent progress in the modeling of frequency comb sources focusing on mode-locked lasers, supercontinuum generation, and microresonators. There is vast amount of literatures on mode-locked lasers alone. In the writing of this review, we found that over 1,300 papers were published in the last ten years with the keyword “mode-locked lasers” in them. The discussion in this paper therefore does not aim to be exhaustive. The topics covered are chosen for coherent presentation of the paper. The rest of the paper is organized as follows. The modeling of mode-locked lasers is discussed in Section 2. Sections 2.1 and 2.2 respectively describe the distributed model and discrete model commonly used to study laser cavities, and the laser configurations described by these models. In Section 2.3, we discuss the limitation of slowly varying envelope approximation, which is used to drive pulse envelope equation in these models, and the short pulse equations which have been proven effective in modeling the ultrafast phenomena the slowly envelope approximation is no longer suitable. How heuristic models based on intuition can be used to enhance laser performance is discussed in Section 2.4, and Section 2.5 describes laser design to overcome the limited gain bandwidth of the rare-earth doped fibers in the realization of few cycle mode-locked fiber lasers. The modeling of supercontinuum generation relevant to frequency comb generation is discussed in Section 3. Section 3.1 gives the well-accepted generalized nonlinear Schrödinger equation, which is used to model SC generation in optical fibers. Section 3.2 gives a brief summary of nonlinear dynamics of SC generation. In Section 3.2, we discuss the properties of SC relevant to its use as frequency comb sources. In Section 3.3, we introduce the modeling of SC

generation in nonlinear waveguides. Section 4 discusses the formation and modeling of Kerr comb microresonators. Section 5 gives the summary and discussion.

## 2 Mode-locked lasers

Mode-locked lasers that generate high-power ultrashort pulses are always desirable in the development of lasers. At the time the self-referenced optical frequency comb was first demonstrated, Kerr lens mode-locked (KLM) solid state lasers especially Ti:sapphire lasers were the only choice to generate ultrashort pulses with less than 100 fs duration and several nanojoule level single pulse energy, which is necessary for coherent supercontinuum generation. Ti:sapphire can provide gain in a wide bandwidth spanning several hundreds of nanometers, which can support oscillations of ultrashort pulses even down to a few cycle of optical waves [25, 26]. Compared to other laser sources, Ti:sapphire lasers are still preferred in laboratories in nonlinear optics experiments including, but not be limited to, generation of coherent supercontinua and self-referenced optical frequency combs, because of their high power and ultrashort pulsewidth [19, 25–27]. Besides Ti:sapphire lasers, KLM solid state lasers based on other gain mediums doped by Nd, Cr, Yb, Tm, and other ions also show high power output but relatively longer pulses [28, 29]. Although KLM solid state lasers have achieved much success in the development of optical frequency comb sources, drawbacks such as weight, bulkiness, environmental sensitivity, difficulty of self-starting, and high costs severely limit their usage outside the laboratories. In contrast, rare-earth-doped fiber lasers, which are compact, lightweight, alignment free, and low cost, are desirable if they can generate laser pulses comparable to that from Ti:sapphire lasers in terms of pulse peak power and duration. Generating high-power ultrashort pulses in fiber laser cavities are more difficult than that in Ti:sapphire laser cavities because of the narrow gain bandwidth, large dispersion, and nonlinearity of optical fibers [30–32]. To achieve high-power ultrashort laser pulse output, various mode-locking schemes include nonlinear polarization evolution (NPE) [33], nonlinear loop mirror (NOLM) [34], semiconductor saturable absorber mirror (SESAM) [35], carbon nanotube (CNT), and graphene saturable absorbers [36] have been adopted. Er, Yb, Tm, and other rare-earth-doped fibers have also been used to generate lasers at different wavelengths.

Since the pulse formation process in the laser cavities with different dispersion, nonlinearity, and gain profiles are very complex, theoretical modeling of the laser dynamics is important to understand the physical mechanisms, optimize the cavity design, capture the nonlinear dynamics and ultimately, design novel laser cavities. In the following, we will review the commonly adopted theoretical models in laser modeling.

### 2.1 Distributed model of laser cavities

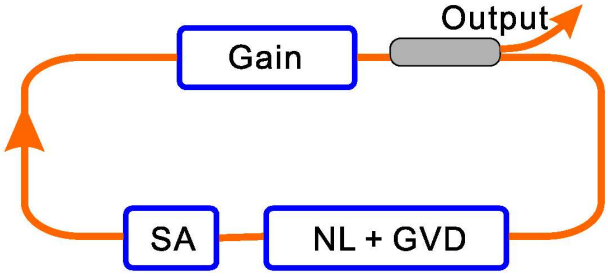


**Figure 2:** Schematic of a mode-locked laser. NL: Nonlinearity, GVD: Group velocity dispersion, SA: Saturable absorber.

Figure 2 shows the schematic of a typical cavity of a mode-locked ring laser. The laser consists of discrete components providing gain, nonlinearity, group velocity dispersion, and saturable absorption. In distributed models of laser cavities, the effect of the discrete components on the circulating light is distributed throughout the cavity such that the pulse evolution in the mode-locked laser can be approximated by a single partial differential equation. The approximation allows the use of analytical techniques to look for pulse solution of the equation. For example, by writing the electric field of the optical signal as $E(z,t) = \psi(z,t)\exp(-i\omega_0 t)$, where $\omega_0$ is the frequency of the optical carrier, and using the slowing varying envelope approximation, the evolution of optical pulses in a mode-locked laser cavity can be described by the quintic complex Ginzburg–Landau equation (QCGLE), which can be written as [37, 38]

$$\begin{aligned} &i\psi_z - \frac{1}{2}\beta_2\psi_{tt} + \gamma|\psi|^2\psi + \varepsilon|\psi|^4\psi \\ &= \frac{i}{2}g(\psi + \eta\psi_{tt}) - \frac{i}{2}\left(\alpha - \mu|\psi|^2 + \nu|\psi|^4\right)\psi, \end{aligned} \tag{1}$$

where $z$ and $t$ are the distance and time variables. The parameter $\beta_2$ is the group velocity dispersion (GVD), $\gamma$ is the Kerr nonlinear coefficient, $\varepsilon$ is the fifth order nonlinear coefficient, $g$ is the gain coefficient, $\alpha$ is the linear loss, and $\eta\psi_{tt}$ describes the gain spectral profile. The terms

$i\mu|\psi|^2\psi$ and $i\nu|\psi|^4\psi$ on the right hand side of (1) represent the response of the mode-locker in the cavity, which can be a saturable absorber or other equivalent effects such as nonlinear polarization rotation. If a fourth-order diffusion term $\kappa\psi_{tttt}$ is added to the QCGLE, it becomes the complex Swift–Hohenberg equation (CSHE), which can be used to model mode-locked lasers with more complex gain profiles [39]. By setting the coefficients $\varepsilon$, and $\nu$ in (1) to zero, the QCGLE is reduced to the well-known Haus's master equation [40].

### 2.1.1 The master equation

The master equation proposed by Haus in the 1970s is a very successful model for mode-locked lasers including KLM solid state lasers and mode-locked fiber lasers [41, 42]. The master equation is the cubic complex Ginzburg–Landau equation (CCGLE), which is given by

$$i\psi_z - \frac{1}{2}\beta_2\psi_{tt} + \gamma|\psi|^2\psi = \frac{i}{2}g(\psi + \eta\psi_{tt}) - \frac{i}{2}\left(\alpha - \mu|\psi|^2\right)\psi. \quad (2)$$

The CCGLE with constant parameters does not possess stable pulse solutions [43] because it does not include gain saturation, which is necessary to avoid the unlimited increase of the pulse energy. The saturation effect of the gain can be determined by a separate equation such as

$$g = \frac{g_0}{1 + E/E_{\text{sat}}}, \quad (3)$$

where the pulse energy $E = \int|\psi|^2 dt$ is integrated in the whole time window.

Equations (2) and (3) can be solved numerically using the split-step Fourier or Runge–Kutta methods [44]. More importantly, the master equation has analytical solutions of the form [40]

$$\psi(t) = x\,\text{sech}^{1+iy}(t/\tau), \quad (4)$$

where $x$, $y$, and $\tau$ are real constants. Stable hyperbolic secant pulse solutions can be obtained in both the anomalous and normal dispersion regions [40, 42]. The typical pulse formation mechanisms in the anomalous and normal dispersion regions, however, are quite different. To illustrate the difference of the pulse dynamics in the two dispersion regions, we qualitatively show the effects of different pulse shaping mechanisms in the two cavities by a series of time frequency maps (TFMs) and differential TFMs in Figure 3. Such time frequency maps can be measured by the frequency resolved optical gating (FROG) technique in experiments or pulse gated time frequency analysis in simulations [45]. In each row of Figure 3, the first figure is the time frequency map of the initial pulse and the other four figures from left to right are the variations induced by self-phase modulation (SPM), GVD, temporal modulation in the saturable absorber, and spectral filtering of the bandwidth limited gain, respectively. The pulse shaping effects on the optical electric field are calculated one by one in the order above in a small fiber segment as the way it would be done in the split-step Fourier simulation of Eq. (2). Then the TFMs before and after the calculation of each pulse shaping effect are compared to obtain the variations caused by each effect, which is shown in the four differential TFMs at each row. In Figure 3, the warm colors (red side) indicate high intensity or intensity increasing and the cool colors (blue side) indicate low intensity or intensity decreasing. Although Figure 3 is not a quantitative representation of the pulse dynamics in any specific laser cavity, the differential TFMs show intuitively the interactions of the various pulse shaping effects in the two dispersion regimes.

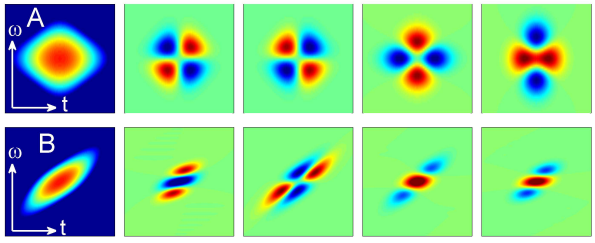


**Figure 3:** The time frequency map evolutions of the pulses in fiber laser cavities with (A) anomalous dispersion and (B) normal dispersion. In each row, the first figure is the time frequency map of the initial pulse and other four figures are the variations induced by SPM, GVD, saturable absorption, and spectral filtering, respectively. The warm colors (red side) indicate high intensity or intensity increasing and the cool colors (blue side) indicate low intensity or intensity decreasing.

In Figure 3A, the first figure shows the TFM of a chirp-free soliton pulse. The symmetry of the TFM implies that the pulse is chirp free. In the following differential TFMs, SPM transfers energy from high frequency to low frequency on the rising edge of the pulse, but from low frequency to high frequency on the falling edge of the pulse. Such energy transfer will induce a positive frequency chirp on the pulse. Anomalous GVD introduces a negative chirp, which can balance the chirp induced from SPM. Such balance is the basis of fundamental soliton formation in passive optical fibers [46]. Saturable absorption, a common mode-locking mechanism, shortens the pulse width and

simultaneously broadens the spectrum of the transform limited pulse. The spectral broadening will then be balanced by spectral filtering as shown in the last differential TFM. The balance between the saturable absorption and the spectral filtering can also be regarded as the balance of the nonlinearity and dispersion of the gain [43]. Clearly, there are two pairs of effects that are mutually balanced to maintain the chirp-free pulse shape in the cavity with anomalous dispersion.

The pulse formation process in normal dispersive cavities is different since SPM and normal dispersion cannot balance each other but jointly stretch the pulse as shown in Figure 3B. SPM will expand the spectrum and normal GVD will enlarge the pulse duration so the pulse trace on the TFM will be stretched along the diagonal direction. In the mode-locking process, the stretching will be compensated by saturable absorption and spectrum filtering [40, 47]. Because the pulse is chirped, the saturable absorption will chop the edges of the pulse in time domain and at the same time narrow the bandwidth. Similarly, chopping the spectrum by spectral filtering will also shorten the pulse in the time domain. The stretching by SPM and GVD in the frequency and time domains balances the compression by saturable absorption and spectral filtering resulting in stable chirp pulse solution [40, 47]. The main advantages of using chirped pulses in the cavity are their low peak power and long pulse duration, which make it possible to support much higher single pulse energy without triggering the wave breaking caused by excessive nonlinear phase accumulation in each round trip [33, 47]. The pulse formation scheme shown in Figure 3B is the basis of most of the techniques that generate high-energy ultrashort pulses from fiber lasers with normal or net-normal dispersion [47].

Besides the balances qualitatively illustrated in Figure 3, the gain loss balance in the cavity is also an important condition for stable pulse lasing. The pulse peak power determined by the gain loss interaction will further affect the nonlinearity in the cavity.

### 2.1.2 QCGLE and dissipative solitons

Although the master equation can successfully model the pulse formation dynamics in both normal and anomalous dispersion regions, the parameter ranges for the existence of stable pulses are relatively narrow [38, 40]. In the master equation, the saturable absorption is modeled by the term $\mu|\psi|^2\psi$, which leads to monotonic increase of the transmittance with the increase of pulse intensity. However, the transmittances of all saturable absorbers, including NOLM, NPE, SESAM, CNT, and graphene, will reach a maximum if the signal intensity is sufficiently large and the transmittance can never be larger than 1. The problem can be solved by introducing high order terms into the CCGLE, which leads to the QCGLE as (1) [48]. Recently, a method was proposed by Ding et al. [49] to include sinusoidal and even arbitrary nonlinear response functions into the CGLE by using their logarithms, which has greatly enhanced the types of lasers that can be modeled by CGLE. An extra benefit of introducing high-order effects is that stable soliton solutions can be found even if the gain is constant [50, 51]. The QCGLE has been discussed thoroughly and extensively not only in optical systems but also many nonequilibrium physical systems to investigate the instabilities [43, 52, 53]. The pulses described by (4) are no longer the analytical solutions of QCGLE. An exact solution of (1) with $\varepsilon = 0$ and $\beta_2 > 0$ is in the form [54]

$$\psi(t,z) = P^{1/2}\left[\cosh(t/\tau) + M\right]^{(ik-1)/2}\exp\left(i\gamma zP/M\right), \quad (5)$$

where $P$, $M$, $\tau$, and $k$ are real constants as described in [54]. Compared with Eq. (4), Eq. (5) is a more general form of the dissipative solitons (DSs) in laser cavities. Figure 4 shows typical DSs with different values of $M$. All the spectra shown in Figure 4 have been observed in experiments [54].

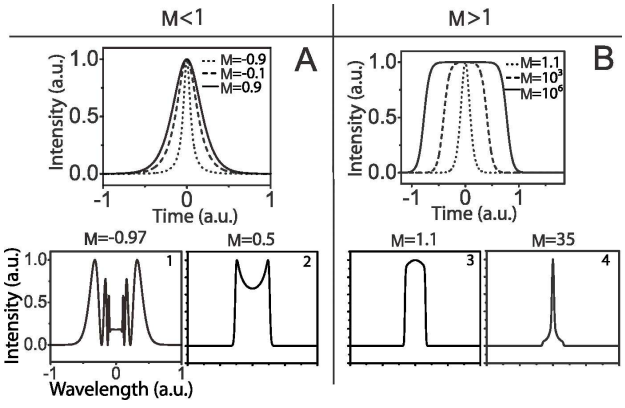


**Figure 4:** The temporal profiles (top) and spectra (bottom) of typical dissipative solitons categorized by the value of $M$. (Adapted from [54]).

From Figure 4, the QCGLE has solutions that cannot be observed in Haus's master equation. A specific example is the chirped bell shape pulse, which is significantly different in shape when compared to the hyperbolic secant pulse [54, 55]. In theory, the bell shape pulse shown in Figure 4B can be infinitely long if the system oscillates near the dissipative soliton resonance [55–57]. Although the analytical solution (5) captures the main features of

the pulses in the cavity, in most cases the parameters range that supports stable numerical solutions does not agree with that from the analytical solution. The parameters range should be searched numerically the efficiency of which can be boosted by using boundary tracking algorithms [58]. Related experiments indicate that DS formed in normal dispersive fiber cavity and compressed outside the cavity is a good candidate of high-energy ultrashort pulses [54]. By using the highly chirped dissipative solitons, mode-locked fiber lasers based on NPE and NOLM in all-normal dispersive (ANDi) single-mode fiber cavities have successfully pushed the single-pulse energy to more than 20 nJ and pulse durations less than 80 fs [33, 55, 59]. A further increase of the single-pulse energy in these single-mode fiber cavities is, however, impeded by practical limitations such as stimulated Raman scattering [60–63].

## 2.2 Discrete model of laser cavities

Distributed models, including Haus's master equation and QCGLE, are very useful in understanding the basic dynamics of pulse evolution in mode-locked lasers. But laser models based on distributed parameters is too qualitative and limited at best because of the assumption that the pulse is near equilibrium when circulating inside the laser cavity. Such models are not effective in describing dispersion managed cavities such as stretched pulse mode-locking [64] and similariton mode-locked cavities [65, 66] in which the laser pulse undergoes large breathing within one round trip [38, 67]. Quantitative modeling of pulse evolution in mode-locked lasers requires the discrete or lump model. In the discrete model, each optical component in the cavity is modeled separately. The optical pulse is modified by each optical component successively when the pulse goes through each round trip in the laser cavity. While the discrete model gives a more realistic description of pulse evolution in the laser cavity, the discrete change in the optical pulse when it moves through the laser cavity make it all but impossible to obtain analytical solutions in such models. Numerical simulations are therefore used almost exclusively to study pulse evolutions described by discrete models.

This is the case even for an all-fiber mode-locked laser. The pulse propagation in a nonlinear, birefringent, and dispersive medium or fibers in general can be modeled by a pair of coupled nonlinear Schrödinger equations [46, 68, 69]:

$$iU_z - \frac{1}{2}\beta_2 U_{tt} - KU + \gamma\left(|U|^2 U + X|V|^2 U + FV^2 U^\star\right) = \frac{i}{2}RU, \quad (6)$$

$$iV_z - \frac{1}{2}\beta_2 V_{tt} + KV + \gamma\left(|V|^2 V + X|U|^2 V + FU^2 V^\star\right) = \frac{i}{2}RV.$$

In (6), $U$ and $V$ respectively represent the slowly varying envelopes of the electric fields in the fiber with orthogonal polarizations along the fast and slow axes of the birefringent fiber with birefringence $K$. The SPM, cross-phase modulation (XPM) and four-wave mixing (FWM) effects are included. In linearly birefringent fibers, the XPM and FWM coefficients $X$ =2/3 and $F$ =1/3 [46]. The terms on the right hand side of (6) model the dissipative effects including the gain and loss with

$$R = \frac{g_0}{1 + E/E_{\text{sat}}}(1 + \eta\partial_{tt}) - \alpha, \quad (7)$$

where the pulse energy is calculated by $E = \int(|U|^2 + |V|^2)dt$. The parameter $\eta$ models the gain bandwidth and $\alpha$ is the linear loss of the fiber. Although (6) and (7) apply to every components of the all-fiber laser, the parameters in different fiber segments can vary significantly. Other optical elements such as wave plates, polarizers, and polarization controllers would be modeled by point functions using Jones matrices [70, 71]. Such a model has been widely used to investigate the pulse solutions in NPE-based mode-locked fiber lasers [70–75]. The stable pulse solutions and nonlinear dynamics of NPE mode-locked lasers are better described by the discrete model (6), when compared to the distributed model. However, exact characterization of fiber parameters, especially random birefringence in experiments, is difficult rendering predictions from the discrete models still qualitative in nature. However, it has been demonstrated that if the random polarization evolution is circumvented by using polarization maintaining fiber in the laser cavity [76–78], the pulse dynamics and output can be accurately predicted by discrete models which include higher order dispersions, self-steepening, and stimulated Raman scattering [61, 79, 80].

### 2.2.1 Dispersion managed mode-locking

A conventional soliton based fiber laser suffers from wave breaking, which is caused by excessive nonlinear phase accumulation because of the high peak power of the ultrashort pulse in the cavity. The single pulse energy is thus limited to ~0.1 nJ [81, 82]. To enhance the pulse energy and narrow the pulse duration from a fiber laser, several cavity designs have been proposed. A dispersion-managed (DM) cavity, which supports stretched pulse oscillation in the cavity, can greatly reduce the effective average power of the

pulse in the cavity by reversing the chirp direction of the pulse twice in each round trip using two segments of fiber with opposite dispersion [64, 83, 84].

Figure 5 shows the typical pulse dynamics in a stretched pulse mode-locked laser cavity obtained with the discrete model [84]. The temporal evolution shown in Figure 5A clearly indicates the pulse compression and stretching in the normal dispersion and anomalous dispersion regions. The pulse duration $T_{RMS}$ has two minima in the cavity as shown in Figure 5B. The chirp $C_{RMS}$ reverses twice in the middle points of the normal and anomalous dispersion regions separately.

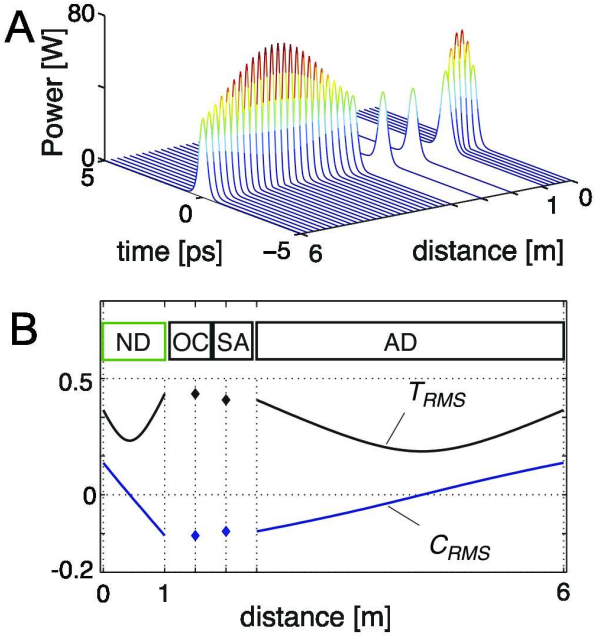


**Figure 5:** The evolutions of the (A) temporal profile, (B) power and chirp during one round trip in a stretched pulse fiber laser cavity. (Adapted from [84]).

With the stretched pulse mode-locking, the single pulse energy can be enhanced to more than 10 nJ [85]. The minimum pulse durations of 25 [27] and 37 fs [86] were obtained with single-mode Yb-doped fiber and Er-doped fiber respectively. The minimum pulse durations are both obtained with pulse energy less than 1 nJ. Wave breaking inside the anomalous dispersive fiber still set the limit on the maximum pulse energy for Er-doped fiber lasers because the peak power can be very large at the points of chirp reversal [84]. This limit is relieved in Yd-doped fiber lasers in which linear anomalous dispersive components such as grating pairs are adopted [85, 87] because no anomalous dispersive single-mode fiber is available at 1.0 μm region. In [85], a single pulse energy of 10 nJ was obtained [47] but further enhancement is limited by the response curve of NPE. We note that the pulse evolution shown in Figure 5 will be different if the operation condition such as the pump power changes. The pulse evolutions may become asymmetric along the fiber, which will shift the $C_{RMS}$ curve in Figure 5 up or down [47, 85].

### 2.2.2 Self-similar mode-locking

In principle, broad spectrum, high pulse energy and low peak power can be obtained simultaneously only with a highly chirped pulse. As discussed in Section 2.1 with the QCGLE, dissipative solitons are used to generate highly chirped high-energy pulses, especially in normal dispersive fiber cavities. Besides modeling with QCGLE, DSs can also be characterized by the discrete model [47, 88, 89]. With the discrete model, different types of DSs and even noise like pulses are observed [88, 89]. In experiments, DSs with 20 nJ single-pulse energy have been demonstrated when a long segment of polarization-maintaining fiber is used in the cavity to reduce the NPE response [60]. But DSs are difficult to be de-chirped especially with high-energy pulses because of the nonlinearity of the chirp and the complex spectral structure [59, 60, 90].

To obtain an ultrashort pulse, the optical spectrum should be sufficiently broad and completely de-chirped to attain a transform limited pulse. If the output pulse of a laser is chirped, then it has to be de-chirped outside the cavity by prisms or grating pairs. However, even with careful design and fine tuning, these components can only compensate the group velocity dispersion and the third order dispersion (TOD) [91, 92]. It is very hard to compress a pulse with complex chirp profile. It is therefore desirable to generate linearly chirped high-energy pulses from mode-locked lasers. Self-similar mode-locked lasers, which have drawn much attention in recent years, are the most promising candidate to generate linearly chirped pulses.

Self-similar propagation of a parabolic pulse in normal dispersive fiber amplifiers [93] are the basis of self-similar mode-locking. In such amplifiers with a constant gain $g$, the parabolic pulses can be described by [93]

$$\psi(z,t) = x\Gamma(z)\sqrt{1-\frac{t^2}{\tau^2\Gamma^2(z)}}\exp\left\{-i\left[\varphi(z)+\frac{gt^2}{6\beta_2}\right]\right\}, \tag{8}$$

where $\Gamma(z) = \exp\left(gz/3\right)$ is the expanding factor, $x$ is the amplitude of the input pulse, and $\tau$ is the pulse duration. In the propagation, the pulse amplitude, duration, and the spectral bandwidth will increase simultaneously by the

factor $\Gamma(z)$. Most important, because of the synchronized increase of the pulse duration, bandwidth, and power, the chirp of the pulse is kept linear during propagation. At the output of the amplifier, the spectrum will be compressed or filtered to narrower bandwidth for the next round trip. The strong filtering by the narrow bandpass filter is the most distinct feature of self-similar mode-locking compared to other mode-locking schemes [94].

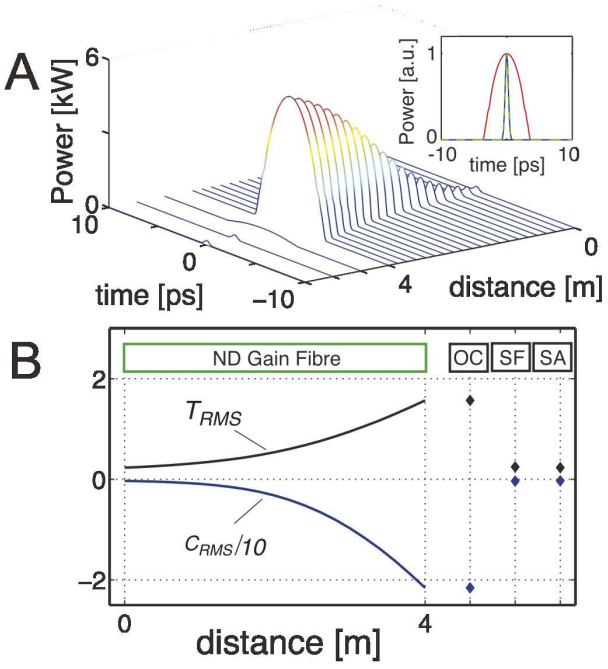


**Figure 6:** The (A) temporal profile, (B) power and chirp evolutions during one round trip in a self-similar fiber laser cavity. (Adapted from [84]).

Figure 6 shows a typical pulse evolution in a self-similar laser. In the normal dispersive gain fiber, the pulse duration $T_{RMS}$ and the chirp factor $C_{RMS}$ both scale exponentially. At the end of the fiber, the spectral filter and saturable absorber chop the pulse to much narrower bandwidth and shorter pulse duration, respectively [95]. The pulse is then injected into the gain fiber again for the next round trip [95]. Self-similar amplification in the cavity enhances the pulse quality. Moreover, because of the large breathing of the pulse power in the cavity, nonlinear phase accumulation is also reduced effectively which in turn enhances the single pulse energy [47, 66]. By adopting self-similar propagation in the gain fiber and using a nonlinear fiber after the gain fiber to further extend the spectrum to over the gain bandwidth limit, such lasers have generated pulse duration about 20 fs, which is currently the record of ultrashort pulse fiber lasers [19, 27, 66]. Detail characterizations of such self-similar fiber lasers can be found in [47] and [84].

Besides using self-similar propagation in the gain fiber, another mode-locking scheme using self-similar propagation in passive fibers was also demonstrated to enhance the pulse energy [33]. In passive self-similar mode-locking, a spectral filter is also adopted in the cavity to increase the pulse bandwidth and duration of breathing. The large breathing of the pulse duration reduced the nonlinear phase accumulation and hence weakened the NPE response limitation [47]. But the chirp profile of the pulse is not controlled to be linear in the laser cavity so that the high-energy pulses can only be compressed to a little less than 200 fs after de-chirping outside the laser cavity [33].

Table 1 compares the characteristics of the models and laser cavities discussed above. The best pulse energy and pulse width reported for each laser cavity configuration using single-mode optical fiber are also provided.

## 2.3 Beyond the slowly varying envelope approximation

The shortest pulses generated by fiber lasers rapidly approach a few optical cycles and those from solid state lasers reach single cycle or even subcycle. The validity of the nonlinear Schrödinger (NLS) family of equations, which are based on the slowly varying envelope approximation (SVEA), comes into question [97–100]. When the pulse contains only few or even less than one optical cycle, the absolute phase and the detail of the wave packet become important [101, 102]. Although it has been shown that the SVEA can be used to describe single-cycle pulse propagation and extreme spectral broadening processes such as SC generation [97, 103], there are considerable ongoing theoretical works on the correction of the SVEA approach [97, 104, 105]. The models beyond the SVEA derived from Maxwell's equation, including the modified Korteweg-de Vries (mKdV), sine-Gordon (sG), mKdV-sG, and short pulse equation (SPE), which is recognized as a reduction of the mKdV-sG [99], have been proven effective in modeling ultrafast phenomena where the NLSE is no longer valid [98, 100, 106, 107]. Here we only introduce the SPE, which is the simplest among those mentioned above. A detailed introduction of these equations can be found in the well-organized review in [99].

Figure 7 illustrates the intrinsic differences between the SVEA- and the SPE-based models. In SVEA-based models, the signal duration is assumed to be long and thus with limited bandwidth located on both sides of the central frequency. From the modeling aspect, the frequency window

**Table 1:** Comparison of different theoretical models and fiber lasers.

| | | Distributed models | | Discrete model | Characteristics of cavity | Pulse parameters |
|---|---|---|---|---|---|---|
| | | Haus's (2) | QCGLE (1) | CVE (6) | | |
| Analytical solution | | ✓ | ✓ | | | |
| Soliton laser | | ✓ | ✓ | ✓ | Anomalous dispersion | <0.1 nJ, ~250 fs [96] |
| CS | CS | | ✓ | ✓ | Net-normal dispersion | 20 nJ, 200 fs [60]<br>3.6 nJ, 80 fs [59] |
| CS | DM | | | ✓ | Large pulse breathing<br>Chirp reverses twice | 10 nJ, 85 fs [85]<br>2.3 nJ, 25 fs [27] |
| CS | SS | | | | All normal dispersion and narrowband filter | 26 nJ, 165 fs [33]<br>1 nJ, 20 fs [19] |

CVE: Coupled vector equations, CS: Chirped soliton, DM: Dispersion managed, SS: Self-similar

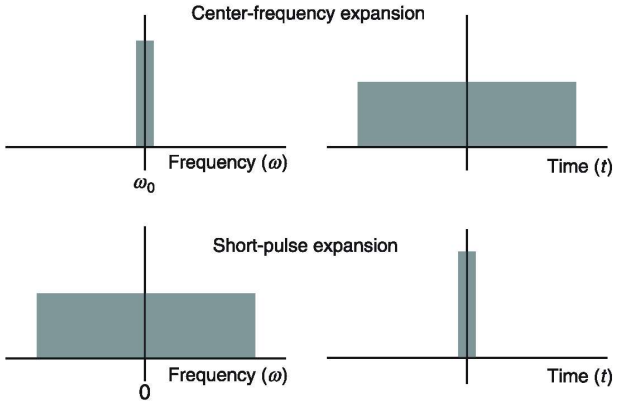


**Figure 7:** Comparison of the SVEA and SPE. (Adapted from [100]).

in SVEA model is limited to less than twice of the carrier frequency or it will extend into the negative frequency and overlap to the spectrum of the conjugate signal. In SPE models, the signal is assumed to be a real delta function in time, which has infinite bandwidth. The spectrum is symmetric and infinitely extendable to model the signal in a very broad frequency window. The normalized SPE master equation to describe the mode-locking can be written as [98–100]

$$u_{zt} - u - \frac{1}{6}(u^3)_{tt} = \left\{ g\mathcal{F}^{-1}\left[f(\omega)\tilde{u}(\omega)\right] - \alpha u + \mu u^3 \right\}_z, \quad (9)$$

where $u(z, t)$ represents the electric field of the optical signal, and $z$ and $t$ are the transformed length and time defined in [100]. The left-hand side of (9) describes the dispersion and nonlinearity and the right-hand side of (9) represents the saturable gain with the profile $f(\omega)$, linear loss $\alpha$ and saturable absorption response $\mu$ of the mode-locker. The function $\mathcal{F}^{-1}[\bullet]$ is the inverse Fourier transform. The definition of $g$ is the same as in (3). Furthermore, the time-dependent response of the third-order susceptibility, which is modeled by the delayed Raman scattering term in the NLSE, can be modeled by replacing the $(u^3)_{tt}$ term as

$$\frac{1}{6}\left(u^3\right)_{tt} \to \frac{1}{6}\left(u\int_0^\infty R(\xi)u^2(z, t-\xi)d\xi\right)_{tt}. \quad (10)$$

Figure 8 shows the evolution from a noise seed to an ultrashort pulse governed by the SPE. The SPE captures the phase dynamics of the electric field, which is important in characterizations of few-cycle to attosecond pulses [99, 100, 102, 107] and mode-locked lasers down to few cycle or subcycle regime [98, 108].

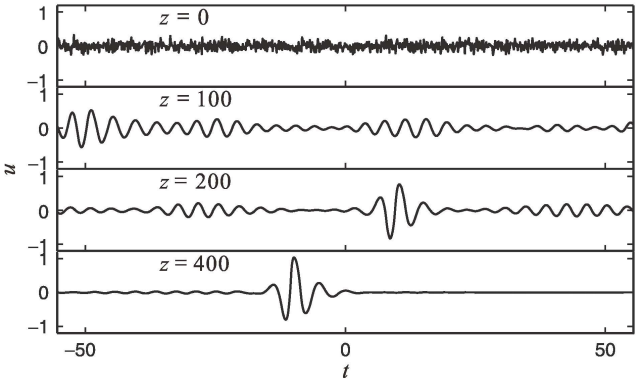


**Figure 8:** Modeling the self-starting of a mode-locked laser with SPE. (Adapted from [100]).

## 2.4 Heuristic models to enhance the performance of mode-locked lasers

Accurate modeling the pulse dynamics and determination of the steady state solutions of a laser cavity provide the understanding, characterization, and possibly a route to enhance the performance of mode-locked lasers. However, it is easy to get lost in the details. Instead of building models that try to mimic the experiments as much as possible, sometimes it is worthwhile to pursue highly simplified heuristic models built from intuition such that the physical mechanisms can be delineated clearly. The lesson learnt can then be used to guide the laser design to enhance the performance, of course only after verification of the results by simulation using more sophisticated models.

High peak power is of critical importance to initiate high-order soliton propagation in a nonlinear fiber for supercontinuum generation [20]. The pulse energy of the laser output determines the peak power of the ultrashort pulse obtained after compression outside the laser cavity. In lasers adopting NPE or NOLM as the modelockers, when wave breaking caused by soliton dynamics is avoided, the periodic nonlinear response of the modelocker becomes the major bottleneck for further increase of the single pulse energy [33, 60, 85, 109].

Figure 9A shows a geometrical description of the multipulsing criterion that includes only the interaction of the gain (red solid lines) and the nonlinear response of NPE/NOLM (blue solid line) [110]. The labels 1, 2, and 3 correspond to gain curves assuming one, two, and three pulses in the cavity, respectively. The operation point of the laser is given by the intersection of the gain and loss curves. When the pump power increases, the gain curve will shift toward the right hand side, thus the pulse energy increases. However, if the laser operation point drops below the small signal response of the nonlinear loss (dashed curves), the pulse will have lower transmittance or higher loss than the small signal in the cavity. The small signal will then be amplified and multipulse lasing will start. After a transition period, the cavity is assumed to support one more pulse. The heuristic model does not describe the dynamics of the transition period, and assume the laser will switch to operating at the gain curve with an additional pulse in the cavity. The highly simplified model provides an intuitive understanding of the multipulsing caused by the gain-loss dynamics, and a guideline to increase the single pulse energy. Different methods to engineer the response curve have been proposed, for example by cascading multiple NPEs or NOLMs [70, 111, 112]. Figure 9B shows the nonlinear loss curve (blue solid line) based on cascading two NPEs. The multipulsing threshold is increased by more than four times. Simulations using the full model (6) and (7) demonstrated nearly thrice enhancement in cavities with cascaded two NPEs [70] or two NOLMs [112].

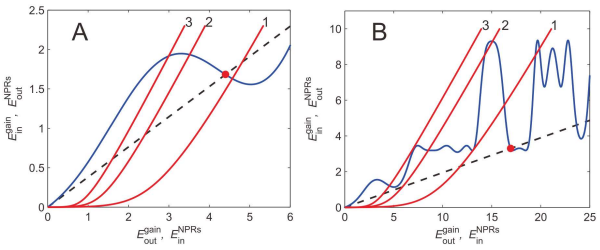


**Figure 9:** (A) Geometrical description of the multipulsing process in mode-locked lasers with saturable gain and nonlinear loss. (B) Enhancement of single-pulse energy by engineering the nonlinear loss curve using two NPEs. (Adapted from [70]).

The multipulsing threshold can also be increased by reducing the fiber cavity length because the oscillation period of the NPE response curve increases when the cavity length decreases. However, short cavity lengths limit the maximum energy that can be acquired from the pump. Inserting a segment of polarization maintained (PM) fiber in the cavity can "freeze" the polarization state in part of the cavity and weaken the NPE response. This method is shown to increase the single pulse energy to 20 nJ, which is comparable to the results of passive self-similar modelocking [33, 60].

## 2.5 Toward few cycle fiber lasers

Unlike Ti:sapphire, other gain media, especially the rare-earth doped silica optical fibers in the near infrared low loss spectral window, have much narrower gain bandwidths, which are typically only several tens of nanometers. This limitation of the gain bandwidth has to be overcome for the generation of few cycle pulses and octave spanning spectra in fiber lasers.

One possible method is to expand the pulse spectrum by nonlinear effects after the gain fiber. Preliminary experiments demonstrates the feasibility by generating 25 and 20 fs pulses directly from stretched pulse [27] and self-similar [19] fiber laser cavities respectively. It is expected that the spectral bandwidth can be further enhanced by improved cavity designs. However, if the expanded spectrum is too broad, the narrowband spectral filter will induce large loss in the cavity, which will upset the gain loss balance. Nonlinear spectral compression adopted in the

cavity to reduce the filtering loss and enhance the power efficiency was proposed theoretically in [113] and experimentally demonstrated in [27]. Spectrum compression in fibers has been discussed for more than two decades [114–116]. The spectrum can be greatly compressed in passive fiber, especially with dispersion increasing fiber to support self-similar spectral compression, which is the inversion of self-similar pulse compression [116–118]. But the fiber length required for large compression ratio is too long for a laser cavity. Recently, we have demonstrated a practical short nonlinearity increasing PCF design for self-similar pulse compression [119], which could be used in laser cavities for both spectral expansion and spectral compression. Figure 10 shows the schematic of such a self-similar mode-locked fiber laser. Laser cavities with high degree of nonlinear spectral expansion and compression are potential candidates for direct generation of few cycle pulses and even octave spanning spectrum in fiber lasers.

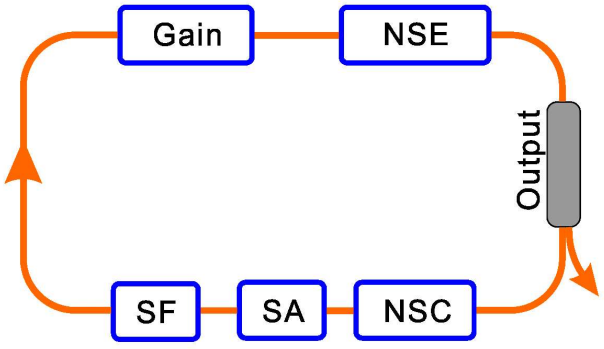


**Figure 10:** Illustration of a self-similar few cycle fiber laser. NSE: Nonlinear spectral expansion, NSC: Nonlinear spectral compression, SA: Saturable absorber, SF: Spectral filter.

# 3 Supercontinuum generation

Optical frequency comb generation, which was cited in the 2005 Nobel Prize in Physics, is only one of the many applications of supercontinuum generation, albeit an important one [2, 120]. SC spectra, which can range from ultraviolet to mid-infrared wavelengths, has many other applications including optical coherence tomography, spectroscopy, microscopy, gas sensing, etc. SC generation has been around since 1970 [121–124]. Here we focus on SC generation since the experiments by J. Ranka et al. in 2000 using a PCF [125]. SC generation in PCFs remains an active research area in the past 15 years. Recently SC generation in high-performance nonlinear waveguides has also attracted much attention [126–129]. Generation of SC is straightforward but its dynamics is rather complex. Numerical modeling of SC generation is instrumental in the understanding of the physics behind the nonlinear dynamics of SC generation. Compared with mode-locked lasers, modeling of SC generation is simpler. Both SC generation in PCF and nonlinear waveguides are well described by the generalized nonlinear Schrödinger equation (GNLSE) with different physical effects included [20, 127, 128], although there has been much discussion on the physical validity of the SVEA used in deriving the GNLSE [97, 104, 105, 130].

## 3.1 SC generation in optical fibers

SC generation in optical fibers can be modeled by the GNLSE [20]

$$\psi(z,T)_z + \frac{1}{2}\alpha\psi - \sum_{k\geq 2} i^{k+1}\frac{1}{k!}\beta_k \psi_T^{(k)} = \tag{11}$$

$$i\gamma\left(1 + i\tau_S \partial_T\right)\left[\psi(z,T)\int_0^\infty R(\xi)\,|\psi(z,T-\xi)|^2 d\xi\right],$$

where the left-hand side of (11) models linear propagation effects and the right-hand side of (11) models nonlinear effects. Here $\psi(z,T)$ is the envelope of the electric field of the optical signal, $\alpha$ is the linear loss, $\beta_k$ is $k$-th order dispersion coefficient associated with the Taylor series expansion of the propagation constant $\beta(\omega)$ at $\omega_0$ where $\omega_0$ is the center frequency. $\gamma$ is the nonlinear coefficient of the fiber, and the self-steepening effect is characterized by a time scale $\tau_s = 1/\omega_0$. $R(\xi)$ is the Raman response function [46].

SC generation is intrinsically a noise sensitive process. Fluctuations of the input pulse significantly affect the stability of the intensity and phase of the SC generated. Numerically, it is common to simulate noise semiclassically by adding a random electric field on each numerical grid point in the frequency domain, i.e., the so-called one-photon-per-mode model [131]. Recently, new models of the input shot noise have been proposed, which take into account the finite linewidth of the pump laser by using a phase-diffusion model [132, 133]. It has been shown that the common one-photon-per-mode model agrees reasonably well with experiments for narrow pump linewidth (< 0.04 nm). On the other hand, the effect of the finite pump linewidth in the noise model should be taken into account if the pump linewidth is broad (> 0.7 nm) [132]. A

combination of the both models gives the best results for pump linewidths in between the two limits.

## 3.2 Dynamics of SC generation

SC has been generated in optical fibers using various optical pump sources through the interaction of fiber nonlinearity and dispersion near the zero dispersion wavelength (ZDW). If the pump is launched in the anomalous dispersion region, the SC generation dynamics can be classified into the soliton fission regime and modulation instability regime.

The first demonstration of SC generation in a PCF operated in the soliton fission regime [125]. In this regime, a high-power ultrashort femtosecond pulse, which can be considered as a higher order soliton of the underlying NLSE, is launched into a PCF or other highly nonlinear fibers. Figure 11 shows the typical evolutions of the spectrum and waveform in SC generation. A 50 fs pulse with 80 kW peak power is injected into a 20 cm nonlinear fiber with a ZDW near 1500 nm. Under the influence of higher order dispersion and nonlinear effects, the high-order soliton undergoes an initial period of spectral broadening and temporal compression, and then breaks up into its constituent distinct fundamental solitons. Soliton fission generated SC has a high degree of temporal coherence [20, 125], and the SC can be generated in a few centimeters of PCF. However, the average power of the SC generated is limited by the availability of high-power pump sources. Also typically, the SC spectrum is not smooth because the fundamental soliton components of the injected femtosecond pulses are distinct and localized.

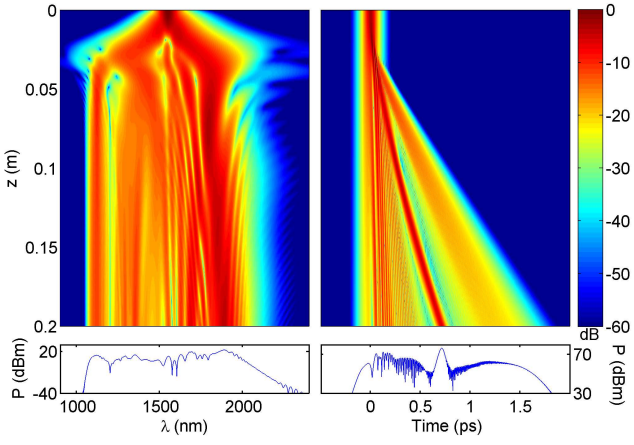


**Figure 11:** Typical spectrum and waveform evolutions in SC generation. A 50 fs pulse with 80 kW peak power is injected into a 20 cm nonlinear fiber with a ZDW near 1500 nm.

The SC can also be generated by launching continuous waves (CW) or quasi-continuous waves into a PCF or highly nonlinear fiber. The injected light is unstable because of modulation instability (MI) and quickly breaks up into a series of fundamental solitons with different energies as MI is a noise-driven process. Similar to the soliton fission regime, these fundamental solitons subsequently shift to longer wavelengths through Raman self-frequency shift when propagating along the fiber. Dispersive waves are also generated on the shorter wavelength side of the ZDW in the process. In general, the long wavelength side of the SC spectra in the MI regime is spectrally smoother when compared to that generated in the fission regime.

Finally, SC can also be generated by launching the pump light into the normal dispersion region. In fact, before the demonstrations of SC generation with pump light in the anomalous dispersion region by Beaud [122] and Islam [123, 124], smooth SC generations in bulk glass [121], or optical fibers [134] are pumped in normal dispersion region because of the lack of pump sources in the anomalous dispersion region then [20, 135]. With pumping in normal dispersion region, the mutual interactions of SPM, XPM, FWM, and Raman scattering jointly expand the spectrum and smooth it by merging the discrete frequency components generated [135–138]. In recent years, SC generations in all normal dispersive fibers without ZDW have been demonstrated. Highly coherent supercontinua with flat spectra are generated in such fibers [139–143]. However, without the tremendous spectral broadening of soliton fission, much higher peak power is required to generate SC with bandwidth comparable to that generated with the anomalous dispersion pump scheme [139–143].

## 3.3 SC as frequency comb sources

The development of low-noise low-cost stable SC-based frequency comb sources requires broadband, flat, and highly coherent SC sources. Numerical simulations of (11) have been used to provide general guidelines in terms of the types of pump source, pump wavelengths, and fiber parameters to generate SC as frequency comb sources.

Frequency comb sources covering as wide a wavelength range as possible is always desirable. SC spectra spanning visible to near-infrared wavelengths in silica-based fibers have been successfully demonstrated. The current focus is to extend into the mid-infrared and the ultraviolet wavelength regions. Here again, modeling of the PCF design optimized for SC generation is playing an important role. However, on the infrared side, the material absorption in fused-silica glass limits the wavelengths

to < 2.5 μm. On the ultraviolet side, solarization-resistant fibers are needed to avoid damage to the silica fibers operating with wavelengths less than ~380 nm.

Spectral flatness can be achieved through engineering of the PCF dispersion and/or nonlinearity properties for SC generation. For example, PCF with longitudinally varying dispersion profile [144, 145] can generate highly coherent flat SC spectra in the picosecond regime.

Figure 12 shows the SC spectra and corresponding moduli of the complex degree of first-order coherence [146] of the SC generated with picosecond pump pulses (Figures 12A and 12C) and with femtosecond pump pulses (Figures 12B and 12D), respectively [119]. Although the SC generated using femtosecond laser pulses are stable and coherent, high-power femtosecond laser sources typically are costly and require careful handling and thus limit the wide applications of these frequency comb sources outside the laboratories. SC generation using picosecond or nanosecond laser pulses are easier to manipulate but the SC generated are unstable and incoherent because of the MI process involved in the generation of the SC. Various methods have been proposed to control the properties of the SC spectra like modification of input laser light and novel design of the PCF. In 2008 Solli et al. first demonstrated that an active scheme using a 200 fs probe pulse with 0.01% of the pump intensity amplitude can greatly enhance the coherence property [147]. Dudley et al. suggested either to add a small 5.8 THz modulation of input pulse or a frequency sliding filter [131]. For SC generation with picosecond pulses, it has been shown both experimentally [148] and numerically [149] that a minute CW trigger enables active control of the SC bandwidth and coherence. The SC coherence property can also be greatly improved by modulating the input pulse with a seed [150]. Various fiber designs have also been proposed to enhance SC coherence. Lu and Knox used dispersion micromanaged holey fiber to shift wavelengths with up to 20 dB lower broadband noise [151]. Optimized solid-core photonic bandgap fibers were also reported to lead to significant reduction of power fluctuations at the long-wavelength edge [152]. Recently, large mode area (LMA) PCF tapers for coherent SC generation was also numerically demonstrated [119].

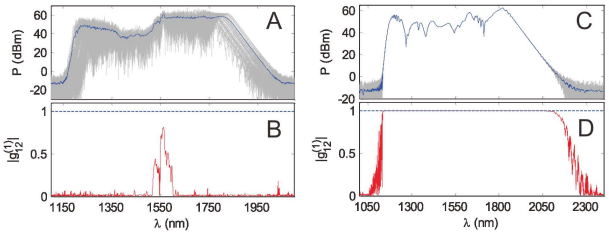


**Figure 12:** (A) and (C) are SC spectra (gray curves are the SCs of individual shots and blue curves are the shot average). (B) and (D) are the corresponding moduli of the complex degree of first-order coherence of the SC. The left column is for the picosecond pump pulse and right column is for the femtosecond pump pulse. (Adapted from [119]).

## 3.4 SC generation in waveguides

Nonlinear waveguides have a number of advantages over optical fibers as compact, on-chip integratable, low-cost, and octave spanning SC-based frequency comb sources. Waveguides formed by highly nonlinear materials, e.g., chalcogenide glasses ($As_2S_3$, $As_2Se_3$, etc.) [153, 154], Group IV semiconductors (silicon, germanium, silicon nitride, silicon nanocrystal, etc.) [155–157], and organics (PTS, etc.) [158], generally show much higher nonlinear refractive indices and larger core-cladding refractive index contrast than silica-based fibers. Thus, strong nonlinear interaction can occur in a small geometrical size (nanoscale) and a short waveguide length (millimeters to centimeters). In a typical silicon-on-insulator (SOI) waveguide, the linear and nonlinear refractive indices of silicon core at 1550 nm are 3.47 and $6 \times 10^{-18}$ $m^2/W$ [159], which are about 2 and 200 times larger than that of the silicon oxide substrate (1.45 and $2.6 \times 10^{-20}$ $m^2/W$). Also, the waveguide dispersion dominates the total dispersion because of the strong mode confinement in the nonlinear waveguides. Thus, flexible dispersion engineering can be achieved by changing the geometrical parameters of the waveguides. The fabrication of most mainstream nonlinear waveguides is compatible with the complementary metal oxide semiconductor (CMOS) process, which allows low-cost on-chip mass manufacturing. The materials of nonlinear waveguides also have larger transparent frequency windows than silica. Thus, the SC generated in the nonlinear waveguides can be extended deeply into the mid-infrared region, which is hard to be achieved by using silica-based fibers. However, some of the materials of nonlinear waveguides have nonlinear absorptions such as multiphoton absorption and free carrier absorption [160, 161]. The nonlinear absorption can degrade the nonlinear performance and should be taken into account when modeling the SC-based comb generation in nonlinear waveguides.

Similar to optical fibers, evolution of the optical pulse train in nonlinear waveguides is governed by the GNLSE but the effects including multiphoton absorption, and free carrier induced absorption and dispersion should be in-

cluded as [162]

$$\psi(z,T)_z = -\frac{1}{2}(\alpha+\alpha_{\mathrm{FCA}})\psi + \frac{i}{c}\omega_0 n_{\mathrm{FCD}}\psi + \sum_{k\geq 2} i^{k+1}\frac{1}{k!}\beta_k\psi_T^{(k)} + \left(i\gamma - \sum_{n=2}^{4}\frac{1}{n}A_{\mathrm{eff}}^{-(n-1)}\beta_{\mathrm{nPA}}|\psi|^{2(n-2)}\right) \times (1+i\tau_s\partial_T)\left[\psi(z,T)\int_0^\infty R(\xi)|\psi(z,T-\xi)|^2 d\xi\right], \quad (12)$$

where $\beta_{\mathrm{nPA}}$ is the $n$-photon absorption coefficients, $\alpha_{\mathrm{FCA}} = \sigma N_c$ and $n_{\mathrm{FCD}} = \zeta N_c$ are the free-carrier absorption (FCA) and free-carrier dispersion (FCD) induced index change respectively [162]. $A_{\mathrm{eff}}$ is the effective mode area. $\sigma$ and $\zeta$ are the free carrier coefficients related to the waveguide materials. $N_c$ is the free carrier density which is given by

$$N_c(z,T)_T = \frac{1}{\hbar f_0}\sum_{n=2}^{4}\frac{\beta_{\mathrm{nPA}}}{nA_{\mathrm{eff}}^n}|\psi(z,T)|^{2n} - \frac{1}{\tau}N_c(z,T), \quad (13)$$

where $\hbar$ is the reduced Planck constant, $f_0 = \omega_0/2\pi$ is the center frequency, and $\tau$ is the free carrier lifetime.

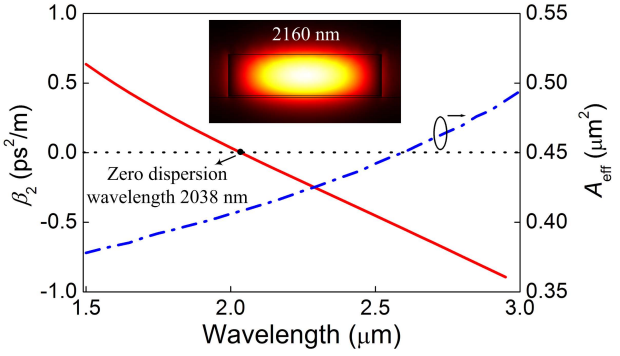


**Figure 13:** Second-order dispersion and effective mode area as a function of the wavelength. Inset: the cross-section of the SOI waveguide and the transverse profiles of the electric field for quasi-TE polarization calculated at 2160 nm.

Figure 13 shows an SOI strip waveguide, which can generate octave-spanning SC combs in mid-infrared region. The waveguide has a 1600 × 430 nm silicon core layer deposited on a 4 × 4 μm buried silicon oxide layer. The 20 nm over etched oxide layer is used to engineer the dispersion of the waveguide. The ZDW is found to be 2038 nm. Since silicon exhibits negligible two- and four-photon absorption in the mid-infrared region, only the three-photon absorption is included in the simulation [163–165].

Since the typical carrier lifetime of silicon is $\tau$ = 1 ns and the pulse width is far less than $\tau$, the free carriers do not have enough time to recombine in the pulse duration. Thus, (13) can be solved analytically by neglecting the $\tau$ term.

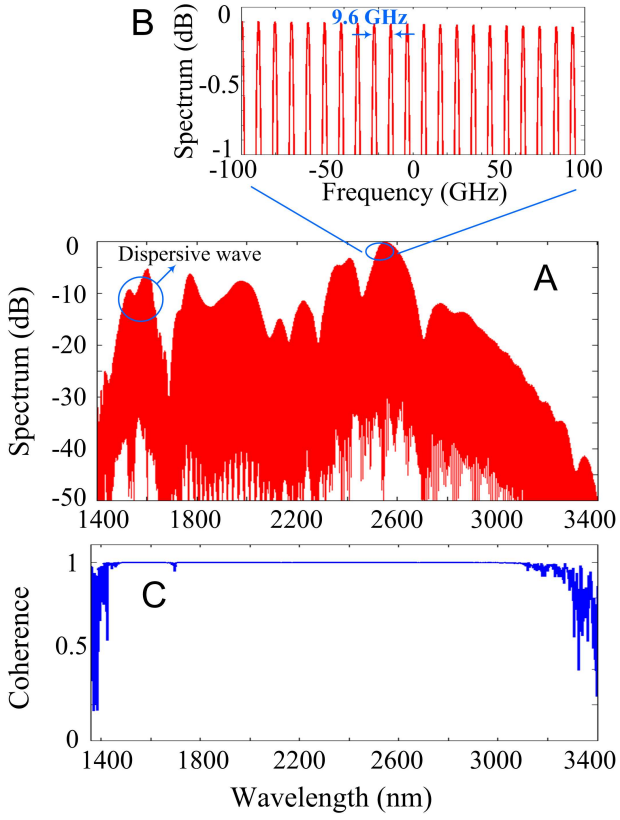


**Figure 14:** (A) The spectral profiles of the pulse train after propagation inside the 1 cm long SOI waveguide, (B) zoom-in view of the spectral component centered at 2520 nm with 200 GHz bandwidth, and (C) the SC coherence as a function of the wavelength. The parameters $\alpha$ = 0.1 dB/cm, $\gamma$ = 45 W$^{-1}$/m, $\beta_{3\mathrm{PA}} = 2.5\times10^{-26}$ m$^3$/W$^2$, $\sigma = 2.77\times10^{-21}$ m$^2$, and $\zeta = -2.7\times10^{-27}$ m$^3$.

Figure 14A shows the spectral profiles of the pulse train after propagation inside 1 cm of the SOI strip waveguide. The pulse train is centered at 2160 nm and assumed to contain 100 pulses with a repetition rate of 9.6 GHz. The peak power and the full width at half maximum (FWHM) of the pulses are 225 W and 50 fs, respectively. The corresponding average power is only 61.3 mW. From Figure 14A, the spectra are greatly broadened from mid-infrared to the telecommunication bands. The −30 dB bandwidth of the generated SC combs cover 1464–3102 nm. The spectral broadening is mainly caused by a combination of the Kerr effect, soliton self-frequency shift, and dispersive wave generation. The dispersive wave is at around 1580 nm, which helps the spectra to spread deeply into the normal dispersion region. Figure 14B shows a zoom-in view of the

comb line structure of the spectra in a 200 GHz frequency range centered at 2520 nm. Figure 14C shows the degree of coherence of the frequency comb versus wavelength. The coherence is close to unity in almost the whole range of the comb except a small degradation around 1696 nm. This degradation is caused by the deep gap of the SC comb spectra at the same wavelength region.

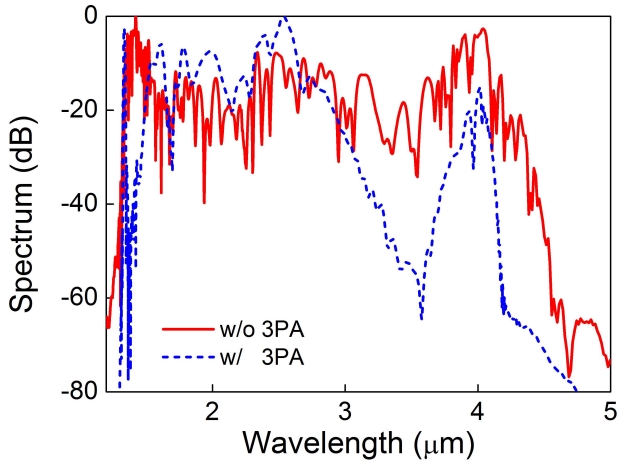


**Figure 15:** The spectral profiles of a single-pulse after propagation inside the 1 cm long SOI waveguide with (dashed line) and without (solid line) 3PA.

Figure 15 shows the spectral profiles of a single pulse at the output of the waveguide with and without three-photon absorption (3PA). It is evident that the effect of 3PA is important particularly in the Stokes-side of the SC. Therefore 3PA should be included in modeling of SC generation in these waveguides.

# 4 Kerr combs

Kerr combs are an important class of optical frequency combs discovered in 2007 [21]. The third-order Kerr effect plays a key role in the generation of both the SC combs and Kerr combs, but the formation mechanisms of them are quite different. Currently, SC-based comb formation requires a high-power ultrashort mode-locked laser as the pump source. A mode-locked laser naturally has a comb feature in frequency domain because the pulses are periodic and discrete in time domain. The function of the SC generator is to further broaden the spectrum to obtain a coherent and octave-spanning comb. In contrast, the Kerr combs exploit parametric frequency conversion in high-Q microresonators [4, 21]. When a CW pump source is coupled into a high-finesse microresonator, the CW light interacts with the modes of the microresonator through the Kerr nonlinearity, and forms the hyperparametric oscillation [22–24, 166]. The mechanism of Kerr comb formation will be further discussed in the next section.

The structures of microresonators are typically microrings with silicon nitride [167–170] or high-index silica [24], micro-disks and micro-spheres with crystalline materials, e.g., fused silica [171, 172], calcium or magnesium fluoride [173–175]. The latter two structures support ultrahigh-$Q$ ($10^6$) whispering gallery modes, which lead to low threshold and more efficient nonlinear interactions inside the microresonators. Resonator-based Kerr comb generators are potential compact, low-cost, and octave-spanning optical frequency comb sources. However, the thermal noise of the CW cavity-stabilized lasers was found to degrade the frequency stability of the combs [176], which limits the applications of the combs and should be resolved with efficient noise suppression techniques.

## 4.1 Formation of Kerr combs

The Kerr comb formation in a nonlinear microresonator is dominated by the hyperparametric oscillation [175, 177], i.e., the combination of modulation instability (MI) and cascaded FWM. Figure 16 illustrates the dynamics of Kerr comb formation. Here, we assume the pump is launched in the anomalous dispersion region, which enables stable and broad comb formation.

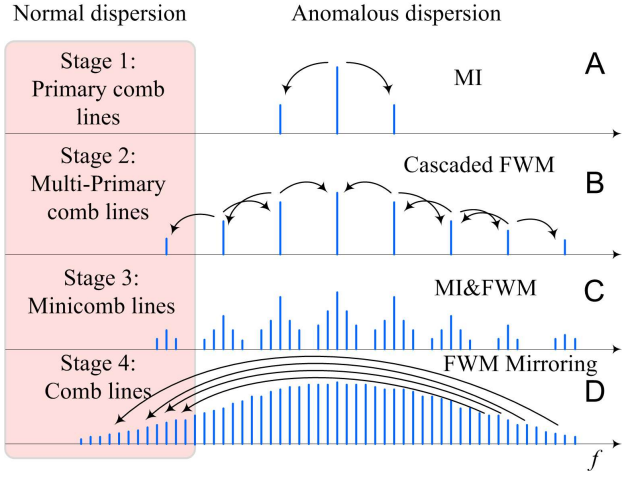


**Figure 16:** The dynamics of Kerr comb formation. (A) Stage 1: primary comb line formation by MI, (B) stage 2: multiprimary comb line formation by cascaded FWM, (C) stage 3: minicomb line formation by combination of MI and cascaded FWM, and (D) stage 4: final comb line formation.

The formation of the Kerr comb can be divided into four main stages as shown in Figure 16 [173, 177, 178]. In stage 1, the energy of the intracavity pump field accumulates with the continuous injection of the CW pump source. When the energy reaches a threshold, the MI gain will overcome the loss of the cavity. Figure 16A shows two primary comb lines symmetrically located on both sides of the pump, which are generated through energy conversion from the pump. The frequencies of the two comb lines follow the phase-matching condition, which are determined by the dispersion of the resonator and the pump power. In contrast to single-pass fiber systems, MI is also found to arise in the normal dispersion region of passive cavities [179, 180]. With further increase of the pump power, the process moves to stage 2 in which cascaded FWM occurs. Figure 16B shows that cascaded FWM drives power conversion among the pump and MI peaks to generate more equally spaced primary comb lines. Such cascaded comb expansion will continue until the nonuniformity of the cavity modes caused by the dispersion of the resonator disrupts it. In stage 3, further combinations of MI and cascaded FWM lead to the formation of minicomb lines in the gaps of the primary comb lines and the pump. Finally, in stage 4, the pump, the primary and mini-comb lines experience further hyper-FWM, and mirror the comb lines into the normal dispersion region to form the whole Kerr comb. Meanwhile, the temporal profiles of the intracavity field evolve from the CW pump to complex pulse waveforms. The waveforms in the cavity can experience modulation, chaotic, multiple pulse, or single pulse states when the frequency detuning of the CW pump from the target resonant mode of the microresonator is varied [181–187]. With properly chosen frequency detuning, a single stable cavity soliton can be obtained when the generated Kerr comb lines are phase synchronized [183] after complex dynamics of collision and merging of the multiple pulses in the cavity [187–189]. More details of Kerr comb formation can be found in [173, 178].

## 4.2 Modeling Kerr combs

Figure 17 shows a typical micro-ring resonator. A CW pump field $\psi_{\text{in}}$ at frequency $\omega_0$ is coherently injected into the resonator cavity via a coupler with a power coupling coefficient $\theta$. When circulating inside the cavity, the envelope of the intracavity electric field at the beginning of the $(m+1)$-th roundtrip can be related to the field at the end of the $m$-th roundtrip with the boundary condition,

$$\psi_{m+1}(0, T) = \theta^{1/2}\psi_{\text{in}} + (1-\theta)^{1/2}\psi_m(L, T)\, e^{i\phi_0}, \qquad (14)$$

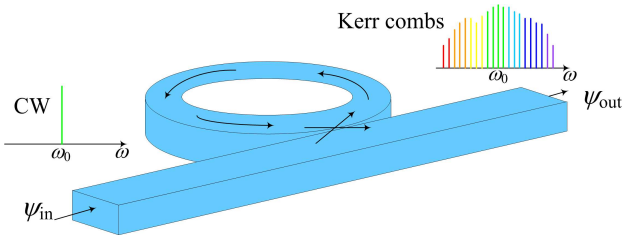


**Figure 17:** Schematic of Kerr comb formation in a micro-ring resonator.

where $m$ is the roundtrip number, $T$ is the temporal time scale of the intracavity field, $L$ is the roundtrip length of the cavity, and $\phi_0$ is the linear phase accumulation of the intracavity field per roundtrip with respect to the pump field. The evolution of $\psi(z, T)\big|_{z=0}^{L}$ in each round trip of the cavity is governed by the NLSE with higher order dispersions and self-steepening,

$$\psi(z, T)_z = -\frac{1}{2}\alpha\psi + i\sum_{k\geq 2} i^k \frac{1}{k!}\beta_k \psi_T^{(k)} + i\gamma\left(1 + i\tau_s\partial_T\right)|\psi|^2\psi, \qquad (15)$$

where $z$ is the propagation distance. $\tau_s$ is the optical shock time and defined as $\tau_s = 1/\omega_0 + (dn_2/d\omega)_{\omega=\omega_0}/n_2 - (dA_{\text{eff}}/d\omega)_{\omega=\omega_0}/A_{\text{eff}}$ [20], which has included the frequency dependence of $n_2$ and $A_{\text{eff}}$ for broadband simulations.

Equations (14) and (15) form an infinite-dimensional Ikeda map [190]. The dynamics of Kerr comb formation inside the resonator can be obtained by directly solving the NLSE (15) with the split-step Fourier method and iterating the results in the boundary condition (14). However, for high finesse resonators, the intracavity field varies very slightly in a single roundtrip because of the ultra-low coupling loss and very short propagation distance. In such cases, (14) and (15) can be averaged to a driven damped NLS-like equation known as the mean-field Lugiato-Lefever equation (LLE) [178, 191]:

$$t_R\psi(t, T)_t = \theta^{1/2}\psi_{\text{in}} - \frac{1}{2}(\alpha L + \theta)\psi + i\left[L\sum_{k\geq 2} i^k \frac{1}{k!}\beta_k \partial_T^{(k)} + \gamma L\left(1 + i\tau_s\partial_T\right)|\psi|^2 - \delta_0\right]\psi, \qquad (16)$$

where $t_R$ =1/FSR is the roundtrip time, FSR is the free spectral range of the resonator, and $t$ is a defined continuous time variable, which measures the slow time of the intra-cavity field evolution. In the strict sense, $t$ has meaning only when it equals to an integer multiple of $t_R$, i.e. $\psi(t = mt_R, T) = \psi_m(L, T)$. In this equation, the fast time $T$ describes the temporal waveform duration localized in

the resonator. The cavity phase detuning $\delta_0 = 2\pi l - \phi_0$ is the phase detuning of the pump field with respect to the closest resonance peak with order $l$.

The LLE was initially used to describe the evolution of spatial structures in passive optical systems [192]. The LLE can be used to describe the dynamics of the signal in microresonators because time can be split to slow time $t$ and fast time $T$ to describe the evolution and the temporal profile of the signal [171, 178, 191, 193–195]. It should be noted that the mean-field LLE is valid only when the following conditions are satisfied. First, the resonator must have high finesse, which is typically $10^4$–$10^9$ for ultrahigh-$Q$ resonators, to keep the intracavity loss low. Secondly, the power coupling coefficient should satisfy $\theta \ll 1$. Finally, the nonlinear length $1/\gamma|\psi|^2$ and the dispersion length $\pi/(\Sigma_{k\geq 2}\beta_k \Delta\omega^k/k!)$, where $\Delta\omega$ is the angular spectral bandwidth of the generated comb, should be much larger than $L$, i.e., the nonlinearity and dispersion inside the cavity are weak. The illustrated model is not limited to the microring resonator, but applies to different resonators structures such as toroid, racetrack, etc.

The steady-state solution of (16) can be obtained by finding the roots of the right-hand side of (16) with the multi-dimensional Newton–Raphson method [191]. Numerical simulations of (16) will capture the dynamics of Kerr comb formation. Figure 18 shows a series of results of the waveforms and spectra in a microresonator pumped by a CW light with different detuning, which are numerically modeled by the LLE in (16). As discussed in Section 4.1, the waveform evolves from quasi-periodic multiple pulses to chaotic quasi-pulses, aperiodic multiple cavity solitons, and finally a single cavity soliton as the pump detuning increases. Besides the variation of waveforms, the spectra of the Kerr comb also vary significantly particularly on the details. When the quasi-periodic multiple pulses are observed in the cavity, the primary comb lines on the spectrum dominate and the mini-comb lines are weak. When the chaotic quasi-pulses and aperiodic solitons are observed, the strengths of the mini-comb lines are comparable to the primary comb lines. To achieve a stable single cavity soliton in the microresonator, the generated Kerr comb lines should be coherent and phase locked as shown by the bottom two plots of Figure 18.

The Kerr comb evolutions shown in Figure 18 demonstrated the ability of LLE to model the dynamics of the temporal profile in microresonators, which helps the understanding of the Kerr comb formation. The accuracy of the LLE shown in (16) can be further improved by including higher order effects such as the Raman scattering when broad spectrum is modeled. Additionally, if the microresonator is fabricated with materials such as silicon, effects

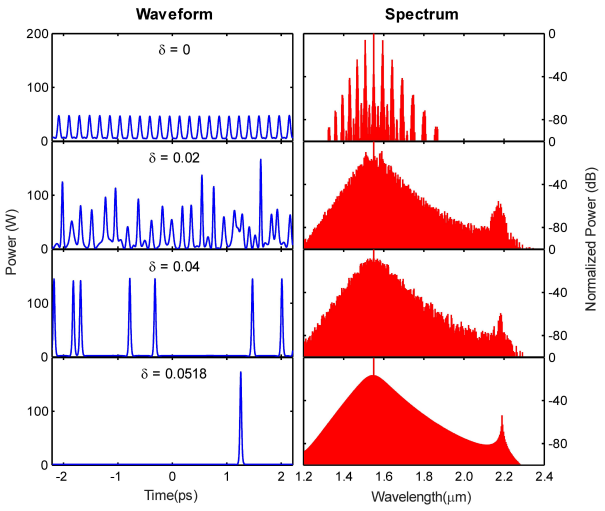


**Figure 18:** The waveforms and spectra of the Kerr comb generated in an $Si_3N_4$ microresonator with a quality factor $Q = 5 \times 10^5$. The round trip time $t_R = 4.425$ ps. $P_{in} = 1.5$ W, $\alpha L = 0.012$, $\theta = 0.0025$, $\gamma = 1\ W^{-1}/m$ and $\beta_2 = -61\ ps^2/km$. The phase detuning $\delta$ increases from 0 to 0.0518 from top to bottom.

such as multiphoton absorption, free-carrier absorption, and dispersion should also be included in the generalized LLE as [196–198]

$$\begin{aligned} t_R\psi(t,T)_t &= \theta^{1/2}\psi_{in} - \left(\frac{1}{2}\alpha L + \frac{1}{2}\theta + i\delta_0\right)\psi \\ &+ \left[iL\sum_{k\geq 2} i^k \frac{1}{k!}\beta_k \partial_T^{(k)} - \frac{1}{2}\alpha_{FCA} + \frac{i}{c}\omega_0 n_{FCD}\right]\psi \\ &+ \left(i\gamma L - L\sum_{n=2}^{4}\frac{1}{n}A_{eff}^{-(n-1)}\beta_{nPA}|\psi|^{2(n-2)}\right) \\ &\times (1 + i\tau_s\partial_T)\left[\psi(t,T)\int_0^\infty R(\xi)|\psi(t,T-\xi)|^2 d\xi\right]. \end{aligned} \tag{17}$$

The definitions of the parameters in (17) are the same as those in (12), (13) and (16) by a change in variable $z \to t$.

Besides the LLE which models the evolution of the temporal profile of all the cavity modes as a whole by a single differential equation, the Kerr comb generation in microresonators can also be modeled by a set of nonlinear coupled mode equations (NCMEs) in which the evolution of each cavity mode is governed by an individual equation as [199, 200]

$$\begin{aligned} \psi_\eta' &= -\frac{1}{2}\Delta\omega_\eta\psi_\eta + \frac{1}{2}\Delta\omega_\eta\delta_{\eta 0}F_0 e^{i\sigma t} \\ &- ig_0\sum_{\alpha,\beta,\mu}\Lambda_\eta^{\alpha\beta\mu}\psi_\alpha\psi_\beta^*\psi_\mu e^{i\varpi_{\alpha\beta\mu\eta}t}, \end{aligned} \tag{18}$$

where the three terms on the right-hand side of (18) represent the linear loss, injected light, and intermodal coupling between different cavity modes, respectively. In (18),

the modal bandwidth $\Delta\omega_\eta$ is inversely proportional to the photon lifetime and describes the decay rate of the photons in mode $\eta$. The Kronecker delta $\delta_{\eta_0}$ indicates the target mode of the external pump light $F_0$ with detuning frequency $\sigma$. $g_0$ is the FWM reference gain and proportional to the nonlinear coefficient. The intermodal coupling factor $\Lambda_\eta^{\alpha\beta\mu}$ defines the coupling strength between the modes $\alpha$, $\beta$, $\mu$, and $\eta$. The frequency detuning $\varpi_{\alpha\beta\mu\eta} = \omega_\alpha - \omega_\beta + \omega_\mu - \omega_\eta$ will determine the phase matching of the FWMs. The NCMEs have also been broadly used in modeling of the spectral evolutions in microresonators [180, 195, 201]. It has been shown that the NCMEs are equivalent to a discrete Fourier expansion of the driven damped NLS equation. Simulation results from the two models agree with each other [183, 195, 202]. The advantage of the NCMEs is the straightforward frequency domain representation and the direct power tracking for each mode. But it is difficult for the NCMEs to include the higher order effects such as self-steepening, Raman scattering, multiphoton absorptions, and free carrier effects, which can be easily modeled using the generalized LLE (17) [202].

# 5 Summary and discussion

In this review, it is difficult not to notice the ubiquitous presence of the nonlinear Schrödinger equation based family of equations. The equations are used to model mode-locked lasers, supercontinuum generation in optical fibers and waveguides, and Kerr comb formation in microresonators. In fact, the NLSE is one of the universal equations that describe the evolution of slowly varying envelope of quasi-monochromatic waves in dispersive weak nonlinear media. Besides nonlinear optics, NLSE serves as a model for nonlinear waves in fluid dynamics from water waves [203] to superfluids [204], Bose–Einstein condensations [205], plasma physics [206], and many others. NLSE is attractive because mathematically it is completely integrable using the inverse scattering transform. Its rich mathematical structure has inspired theoretical studies for many years. Analytical solutions of variants of the NLSE, when available, elucidate the physical phenomena modeled by the equations. When analytical solutions are not available or too complex for practical applications, numerical simulation of the NLS-family of equations using the split-step Fourier method is straight forward allowing detail study of the evolution dynamics. The accessibility of NLS-family of equations by both analytical means and numerical simulation make for fruitful exploration of the physical phenomena modeled by them.

In mode-locked lasers, a variety of laser models have been developed. There are different approaches to modeling serving different purposes. Some researchers treat modeling tools as virtual experiments and try to include as many physical effects as possible in their models. Their goal is to develop as realistic a representation of the real experiments in the models as possible so that predictions from the models will be quantitatively close to the experimental results. Some use modeling to delineate the contribution of various physical effects on an observed phenomenon. Although the results from these typically simplified or reduced models are qualitative, they could provide guidelines and direction in the design of experiments. There are yet others who choose to work in the regime of physical parameters such that the resulting models admit analytical solutions. Despite the limitation of the applicability of the analytical solutions arisen from the compromises made in arriving at such models, these analytical solutions provide understandings and insights that are not possible through numerical simulation of limited regions of the parameter space of the model. No one single modeling approach is superior to the others. Which approach to adopt depends on what one wants to get out from the model.

Rare-earth doped fiber lasers are an attractive candidate of stable, low-cost, and high-quality frequency comb sources either directly as few cycle mode-locked lasers or indirectly as input for SC generation in PCFs or nonlinear waveguides. However, the performance of mode-locked fiber lasers is still inferior to that of their solid state counterpart in terms of peak power and pulse width. Here theory and modeling could play an important role. A combination of the various models would facilitate the development of laser design heuristics, understanding the dynamics of novel laser designs, and assessment of the laser performance. The design freedom of PCFs and waveguides can be used to tailor the dispersion and nonlinear properties for the realization of special pulse evolution characteristics predicted from the models.

Despite the success of the slowly varying envelope approximation in modeling the evolution of few cycle pulses or extreme spectral broadening in supercontinuum generation so far, it is necessary to adopt models that are capable of describing the absolute phase and the detail of the wave packets when the pulses contain only few or even less than one optical cycle. It is of particular interest to develop a unified model that could transform smoothly from the slowly varying envelop approximation to the short pulse limit when an optical pulse is compressed from hundreds of optical cycles down to few or even one cycle either inside a laser cavity or in a specially made fiber.

Finally, the CMOS compatibility of mainstream nonlinear waveguides provides design flexibility and control of fabrication that is not accessible to even photonic crystal fibers. Using microresonators to generate Kerr combs as optical frequency comb sources is surely just the beginning. Other ingenious nonlinear waveguide based methods exploiting other physical mechanisms are likely to be invented in future. Theory and modeling will be indispensable in the development of stable, low-cost, high-quality, on-chip frequency comb sources too.

**Acknowledgement:** We thank Prof. J. Nathan Kutz for the helpful discussions. The work is partly supported by the National Natural Science Foundation of China (61475131, 61307109, and 61307051), the Hong Kong Research Grants Council (PolyU5263/13E and PolyU5272/12E) and the Hong Kong Scholars Program 2013 (PolyU G-YZ45) of the Hong Kong Special Administrative Region of China, the Natural Science Foundation of Beijing (4152037), the Fund of State Key Laboratory of Information Photonics and Optical Communications (Beijing University of Posts and Telecommunications, IPOC2015ZC06) of China and the Beijing Youth Top-notch Talent Support Program (2015000026833ZK08).

## References

[1] Jones DJ, Diddams SA, Ranka JK, et al. Carrier-envelope phase control of femtosecond mode-locked lasers and direct optical frequency synthesis. Science 2000; 288:635–9.
[2] Udem T, Holzwarth R, Hänsch TW. Optical frequency metrology. Nature 2002; 416:233–7.
[3] Diddams SA, Bergquist JC, Jefferts SR, Oates CW. Standards of time and frequency at the outset of the 21st century. Science 2004; 306:1318–24.
[4] Schliesser A, Picqué N, Hänsch TW. Mid-infrared frequency combs. Nat Photon 2012; 6:440–9.
[5] Hänsch TW, Picqué N. Laser spectroscopy and frequency combs. JPCS 2013; 467:012001.
[6] Telle HR, Steinmeyer G, Dunlop AE. Carrier-envelope offset phase control: A novel concept for absolute optical frequency measurement and ultrashort pulse generation. Appl Phys B 1999; 69:327–32.
[7] Cundiff ST. Phase stabilization of ultrashort optical pulses. J Phys D: Appl Phys 2002; 35:R43–R59.
[8] Morgner U, Ell R, Metzler G, et al. Nonlinear optics with phase-controlled pulses in the sub-two-cycle regime. Phys Rev Lett 2001; 86:5462–5.
[9] Ramond TM, Diddams SA, Hollberg L, Bartels A. Phase-coherent link from optical to microwave frequencies by means of the broadband continuum from a 1-GHz Ti:sapphire femtosecondoscillator. Opt Lett 2002; 27:1842–4.
[10] Hitachi K, Ishizawa A, Nishikawa T, Asobe M, Sogawa T. Carrier-envelope offset locking with a 2f-to-3f self-referencing interferometer using a dual-pitch PPLN ridge waveguide. Opt Express 2014; 22:1629–35.
[11] Udem T, Reichert J, Holzwarth R, Hänsch TW. Absolute Optical Frequency Measurement of the Cesium D1 Line with a Mode-Locked Laser. Phys Rev Lett 1999; 82:3568–71.
[12] Reichert J, Holzwarth R, Udem T, Hänsch TW. Measuring the frequency of light with mode-locked lasers. Opt Commun 1999; 172:59–68.
[13] Jones DJ, Cundiff ST, Fortier TM, Hall JL, Ye J. Carrier-envelope phase stabilization of single and multiple femtosecond lasers. in F. X. Kartner, ed. Few-Cycle Laser Pulse Generation and Its Applications. Springer-Verlag Berlin Heidelberg, 2004, 317–43.
[14] Yu TJ, Nam CH. Carrier-envelope phase stabilization of femtosecond lasers by the direct locking method. Prog Quantum Electron 2012; 36:541–65.
[15] Cundiff ST, Ye J. Colloquium: Femtosecond optical frequency combs. Rev Mod Phys 2003; 75:325–42.
[16] Ye J, Cundiff ST. Femtosecond optical frequency comb: Principle, Operation and Applications. Norwell, MA, Springer US, 2005.
[17] Diddams SA. The evolving optical frequency comb [Invited]. J Opt Soc Am B 2010; 27:B51–B62.
[18] Ell R, Morgner U, Kärtner FX, et al. Generation of 5-fs pulses and octave-spanning spectra directly from a Ti:sapphire laser. Opt Lett 2001; 26:373–5.
[19] Chong A, Liu H, Nie B, et al. Pulse generation without gain-bandwidth limitation in a laser with self-similar evolution. Opt Express 2012; 20:14213–20.
[20] Dudley JM, Genty G, Coen S. Supercontinuum generation in photonic crystal fiber. Rev Mod Phys 2006; 78:1135–84.
[21] Del'Haye P, Schliesser A, Arcizet O, Wilken T, Holzwarth R, Kippenberg TJ. Optical frequency comb generation from a monolithic microresonator. Nature 2007; 450:1214–7.
[22] Savchenkov AA, Matsko AB, Strekalov D, Mohageg M, Ilchenko VS, Maleki L. Low threshold optical oscillations in a whispering gallery mode $CaF_2$ resonator. Phys Rev Lett 2004; 93:243905.
[23] Agha IH, Okawachi Y, Gaeta AL. Theoretical and experimental investigation of broadband cascaded four-wave mixing in high-Q microspheres. Opt Express 2009; 17:16209–15.
[24] Razzari L, Duchesne D, Ferrera M, et al. CMOS-compatible integrated optical hyper-parametric oscillator. Nat Photon 2010; 4:41–5.
[25] Morgner U, Kärtner FX, Cho SH, et al. Sub-two-cycle pulses from a Kerr-lens mode-locked Ti:sapphire laser. Opt Lett 1999; 24:411–3.
[26] Brabec T, Krausz F. Intense few-cycle laser fields: frontiers of nonlinear optics. Rev Mod Phys 2000; 72:545–91.
[27] Lan Y, Song Y, Hu M, Liu B, Chai L, Wang C. Enhanced spectral breathing for sub-25 fs pulse generation in a Yb-fiber laser. Opt Lett 2013; 38:1292–4.
[28] Kärtner FX, Morgner U, Schibli T, et al. Few-cycle pulses directly from a laser. in F. X. Kärtner, ed. Few-Cycle Laser Pulse Generation and Its Applications. Springer-Verlag Berlin Heidelberg, 2004, 73–136.
[29] Koechner W. Solid-state laser engineering. New York, USA, Springer New York, 2006.
[30] Fermann ME, Hartl I. Ultrafast fiber laser technology. IEEE J Sel Topics Quantum Electron 2009; 15:191–206.
[31] Richardson DJ, Nilsson J, Clarkson WA. High power fiber lasers: current status and future perspectives [Invited]. J Opt Soc Am B 2010; 27:B63–B92.

[32] Fermann ME, Hartl I. Ultrafast fibre lasers. Nat Photon 2013; 7:868–74.
[33] Chong A, Renninger WH, Wise FW. All-normal-dispersion femtosecond fiber laser with pulse energy above 20 nJ. Opt Lett 2007; 32:2408–10.
[34] Zhao LM, Bartnik AC, Tai QQ, Wise FW. Generation of 8 nJ pulses from a dissipative-soliton fiber laser with a nonlinear optical loop mirror. Opt Lett 2013; 38:1942–4.
[35] Li X, Zou W, Chen J. 41.9 fs hybridly mode-locked Er-doped fiber laser at 212 MHz repetition rate. Opt Lett 2014; 39:1553–6.
[36] Martinez A, Sun Z. Nanotube and graphene saturable absorbers for fibre lasers. Nat Photon 2013; 7:842–5.
[37] Akhmediev N, Ankiewicz A. Dissipative solitons in the complex Ginzburg-Landau and Swift-Hohenberg equations. in N. Akhmediev, and A. Ankiewicz, eds. Dissipative solitons. Springer Berlin Heidelberg, 2005, 17–34.
[38] Kutz JN. Mode-locked soliton lasers. SIAM review 2006; 48:629–78.
[39] Soto-Crespo JM, Akhmediev N. Composite solitons and two-pulse generation in passively mode-locked lasers modeled by the complex quintic Swift-Hohenberg equation. Phys Rev E 2002; 66:066610.
[40] Haus HA, Fujimoto JG, Ippen EP. Structures for additive pulse mode locking. J Opt Soc Am B 1991; 8:2068–76.
[41] Haus HA, Fujimoto JG, Ippen EP. Analytic theory of additive pulse and Kerr lens mode locking. IEEE J Quantum Electron 1992; 28:2086–96.
[42] Haus HA. Mode-locking of lasers. IEEE J Sel Topics Quantum Electron 2000; 6:1173–85.
[43] Akhmediev N, Ankiewicz A. Solitons of the complex Ginzburg-Landau equation. in S. Trillo, and W. Torruellas, eds. Spatial Solitons. Springer-Verlag Berlin Heidelberg, 2001, 311–41.
[44] Wang S, Docherty A, Marks BS, Menyuk CR. Comparison of numerical methods for modeling laser mode locking with saturable gain. J Opt Soc Am B 2013; 30:3064–74.
[45] Trebino R, Delong KW, Fittinghoff DN, et al. Measuring ultrashort laser pulses in the time-frequency domain using frequency-resolved optical gating. Rev Sci Instrum 1997; 68:3277–95.
[46] Agrawal GP. Nonlinear Fiber Optics (Fifth Edition). Boston, Academic Press, 2013.
[47] Renninger W, Chong A, Wise FW. Pulse shaping and evolution in normal-dispersion mode-locked fiber lasers. IEEE J Sel Topics Quantum Electron 2012; 18:389–98.
[48] Moores JD. On the Ginzburg-Landau laser mode-locking model with fifth-order saturable absorber term. Opt Commun 1993; 96:65–70.
[49] Ding E, Shlizerman E, Kutz JN. Generalized master equation for high-energy passive mode-locking: the sinusoidal Ginzburg-Landau equation. IEEE J Quantum Electron 2011; 47:705–14.
[50] Akhmediev NN, Afanasjev VV, Soto-Crespo JM. Singularities and special soliton solutions of the cubic-quintic complex Ginzburg-Landau equation. Phys Rev E 1996; 53:1190–201.
[51] Soto-Crespo JM, Akhmediev NN, Afanasjev VV. Stability of the pulselike solutions of the quintic complex Ginzburg–Landau equation. J Opt Soc Am B 1996; 13:1439–49.
[52] van Saarloos W, Hohenberg PC. Fronts, pulses, sources and sinks in generalized complex Ginzburg-Landau equations. Physica D 1992; 56:303–67.
[53] Marcq P, Chaté H, Conte R. Exact solutions of the one-dimensional quintic complex Ginzburg-Landau equation. Physica D 1994; 73:305–17.
[54] Renninger WH, Chong A, Wise FW. Dissipative solitons in normal-dispersion fiber lasers. Phys Rev A 2008; 77:023814.
[55] Grelu P, Akhmediev N. Dissipative solitons for mode-locked lasers. Nat Photon 2012; 6:84–92.
[56] Chang W, Ankiewicz A, Soto-Crespo JM, Akhmediev N. Dissipative soliton resonances. Phys Rev A 2008; 78:023830.
[57] Grelu P, Chang W, Ankiewicz A, Soto-Crespo JM, Akhmediev N. Dissipative soliton resonance as a guideline for high-energy pulse laser oscillators. J Opt Soc Am B 2010; 27:2336–41.
[58] Wang S, Docherty A, Marks BS, Menyuk CR. Boundary tracking algorithms for determining of the stability of mode locked pulses. J Opt Soc Am B 2014; 31:2914–30.
[59] Mortag D, Wandt D, Morgner U, Kracht D, Neumann J. Sub-80-fs pulses from an all-fiber-integrated dissipative-soliton laser at 1 μm. Opt Express 2011; 19:546–51.
[60] Kharenko DS, Podivilov EV, Apolonski AA, Babin SA. 20 nJ 200 fs all-fiber highly chirped dissipative soliton oscillator. Opt Lett 2012; 37:4104–6.
[61] Aguergaray C, Runge A, Erkintalo M, Broderick NGR. Raman-driven destabilization of mode-locked long cavity fiber lasers: fundamental limitations to energy scalability. Opt Lett 2013; 38:2644–6.
[62] North T, Rochette M. Raman-induced noiselike pulses in a highly nonlinear and dispersive all-fiber ring laser. Opt Lett 2013; 38:890–2.
[63] Runge AFJ, Aguergaray C, Broderick NGR, Erkintalo M. Raman rogue waves in a partially mode-locked fiber laser. Opt Lett 2014; 39:319–22.
[64] Haus HA, Tamura K, Nelson LE, Ippen EP. Stretched-pulse additive pulse mode-locking in fiber ring lasers: theory and experiment. IEEE J Quantum Electron 1995; 31:591–8.
[65] Oktem B, Ülgüdür C, Ilday FÖ. Soliton-similariton fibre laser. Nat Photon 2010; 4:307–11.
[66] Nie B, Pestov D, Wise FW, Dantus M. Generation of 42-fs and 10-nJ pulses from a fiber laser with self-similar evolution in the gain segment. Opt Express 2011; 19:12074–80.
[67] Zaviyalov A, Iliew R, Egorov O, Lederer F. Lumped versus distributed description of mode-locked fiber lasers. J Opt Soc Am B 2010; 27:2313–21.
[68] Menyuk CR. Pulse propagation in an elliptically birefringent Kerr medium. IEEE J Quantum Electron 1989; 25:2674–82.
[69] Chen CJ, Wai PKA, Menyuk CR. Soliton fiber ring laser. Opt Lett 1992; 17:417–9.
[70] Li F, Ding E, Kutz JN, Wai PKA. Dual transmission filters for enhanced energy in mode-locked fiber lasers. Opt Express 2011; 19:23408–19.
[71] Ding E, Renninger WH, Wise FW, Grelu P, Shlizerman E, Kutz JN. High-energy passive mode-locking of fiber lasers. Int J Opt 2012; 2012:354156.
[72] Leblond H, Salhi M, Hideur A, Chartier T, Brunel M, Sanchez F. Experimental and theoretical study of the passively mode-locked ytterbium-doped double-clad fiber laser. Phys Rev A 2002; 65:063811.
[73] Salhi M, Leblond H, Sanchez F. Theoretical study of the erbium-doped fiber laser passively mode-locked by nonlinear polarization rotation. Phys Rev A 2003; 67:013802.
[74] Martel G, Chédot C, Hideur A, Grelu P. Numerical maps for fiber lasers mode locked with nonlinear polarization evolution: comparison with semi-analytical models. Fiber Integr Opt 2008;

27:320–40.
[75] Kobtsev S, Smirnov S, Kukarin S, Turitsyn S. Mode-locked fiber lasers with significant variability of generation regimes. Opt Fiber Technol 2014; 20:615–20.
[76] Aguergaray C, Broderick NGR, Erkintalo M, Chen JSY, Kruglov V. Mode-locked femtosecond all-normal all-PM Yb-doped fiber laser using a nonlinear amplifying loop mirror. Opt Express 2012; 20:10545.
[77] Erkintalo M, Aguergaray C, Runge A, Broderick NGR. Environmentally stable all-PM all-fiber giant chirp oscillator. Opt Express 2012; 20:22669.
[78] Aguergaray C, Hawker R, Runge AFJ, Erkintalo M, Broderick NGR. 120 fs, 4.2 nJ pulses from an all-normal-dispersion, polarization-maintaining, fiber laser. Appl Phys Lett 2013; 103.
[79] Runge AFJ, Aguergaray C, Provo R, Erkintalo M, Broderick NGR. All-normal dispersion fiber lasers mode-locked with a nonlinear amplifying loop mirror. Opt Fiber Technol 2014; 20:657–65.
[80] Runge AFJ, Broderick NGR, Erkintalo M. Observation of soliton explosions in a passively mode-locked fiber laser. Optica 2015; 2:36–9.
[81] Nelson LE, Jones DJ, Tamura K, Haus HA, Ippen EP. Ultrashort-pulse fiber ring lasers. Appl Phys B 1997; 65:277–94.
[82] Town GE, Akhmediev NN, Soto-Crespo JM. Optical fiber soliton lasers. in K. Porsezian, and V. C. Kuriakose, eds. Optical Solitons. Springer Berlin Heidelberg, 2002, 265–97.
[83] Tamura K, Ippen EP, Haus HA. Pulse dynamics in stretched-pulse fiber lasers. Appl Phys Lett 1995; 67:158–60.
[84] Turitsyn SK, Bale BG, Fedoruk MP. Dispersion-managed solitons in fibre systems and lasers. Phys Rep 2012; 521:135–203.
[85] Buckley JR, Wise FW, Ilday FÖ, Sosnowski T. Femtosecond fiber lasers with pulse energies above 10 nJ. Opt Lett 2005; 30:1888–90.
[86] Ma D, Cai Y, Zhou C, Zong W, Chen L, Zhang Z. 37.4 fs pulse generation in an Er:fiber laser at a 225 MHz repetition rate. Opt Lett 2010; 35:2858–60.
[87] Ilday FÖ, Buckley J, Kuznetsova L, Wise FW. Generation of 36-femtosecond pulses from a ytterbium fiber laser. Opt Express 2003; 11:3550–4.
[88] Cheng Z, Li H, Wang P. Simulation of generation of dissipative soliton, dissipative soliton resonance and noise-like pulse in Yb-doped mode-locked fiber lasers. Opt Express 2015; 23:5972–81.
[89] Zhang H, Zhang S, Li X, Han M. Optimal design of higher energy dissipative-soliton fiber lasers. Opt Commun 2015; 335:212–7.
[90] Im JH, Choi SY, Rotermund F, Yeom D-I. All-fiber Er-doped dissipative soliton laser based on evanescent field interaction with carbon nanotube saturable absorber. Opt Express 2010; 18:22141–6.
[91] Buckley JR, Clark SW, Wise FW. Generation of ten-cycle pulses from an ytterbium fiber laser with cubic phase compensation. Opt Lett 2006; 31:1340–2.
[92] Zhou X, Yoshitomi D, Kobayashi Y, Torizuka K. Generation of 28-fs pulses from a mode-locked ytterbium fiber oscillator. Opt Express 2008; 16:7055–9.
[93] Kruglov VI, Peacock AC, Harvey JD, Dudley JM. Self-similar propagation of parabolic pulses in normal-dispersion fiber amplifiers. J Opt Soc Am B 2002; 19:461–9.
[94] Bale BG, Wabnitz S. Strong spectral filtering for a mode-locked similariton fiber laser. Opt Lett 2010; 35:2466–8.
[95] Renninger WH, Chong A, Wise FW. Self-similar pulse evolution in an all-normal-dispersion laser. Phys Rev A 2010; 82:021805(R).
[96] Tamura K, Nelson LE, Haus Ha, Ippen EP. Soliton versus nonsoliton operation of fiber ring lasers. Appl Phys Lett 1994; 64:149–51.
[97] Genty G, Kinsler P, Kibler B, Dudley JM. Nonlinear envelope equation modeling of sub-cycle dynamics and harmonic generation in nonlinear waveguides. Opt Express 2007; 15:5382–7.
[98] Farnum ED, Kutz JN. Master mode-locking theory for few-femtosecond pulses. Opt Lett 2010; 35:3033–5.
[99] Leblond H, Mihalache D. Models of few optical cycle solitons beyond the slowly varying envelope approximation. Phys Rep 2013; 523:61–126.
[100] Kutz JN, Farnum E. Solitons and ultra-short optical waves: the short-pulse equation versus the nonlinear Schrödinger equation. in H. E. Hernández-Figueroa, E. Recami, and M. Zamboni-Rached, eds. Non-Diffracting Waves. Wiley-VCH Verlag GmbH & Co. KGaA, Weinheim, Germany, 2014, 451–71.
[101] Hentschel M, Kienberger R, Spielmann C, et al. Attosecond metrology. Nature 2001; 414:509–13.
[102] Krausz F, Ivanov M. Attosecond physics. Rev Mod Phys 2009; 81:163–234.
[103] Karasawa N, Nakamura S, Nakagawa N, et al. Comparison between theory and experiment of nonlinear propagation for a-few-cycle and ultrabroadband optical pulses in a fused-silica fiber. IEEE J Quantum Electron 2001; 37:398–404.
[104] Kolesik M, Wright EM, Moloney JV. Simulation of femtosecond pulse propagation in sub-micron diameter tapered fibers. Appl Phys B 2004; 79:293–300.
[105] Tyrrell JCA, Kinsler P, New GHC. Pseudospectral spatial-domain: a new method for nonlinear pulse propagation in the few-cycle regime with arbitrary dispersion. J Mod Opt 2005; 52:973–86.
[106] Leblond H, Mihalache D. Few-optical-cycle solitons: Modified Korteweg-de Vries sine-Gordon equation versus other non-slowly-varying-envelope-approximation models. Phys Rev A 2009; 79:063835.
[107] Leblond H, Grelu P, Mihalache D. Models for supercontinuum generation beyond the slowly-varying-envelope approximation. Phys Rev A 2014; 90:053816.
[108] Farnum ED, Kutz JN. Dynamics of a low-dimensional model for short pulse mode locking. Photonics 2015; 2:865–82.
[109] Ilday FÖ, Buckley JR, Lim H, Wise FW, Clark WG. Generation of 50-fs, 5-nJ pulses at 1.03 μm from a wave-breaking-free fiber laser. Opt Lett 2003; 28:1365–7.
[110] Li F, Wai PKA, Kutz JN. Geometrical description of the onset of multi-pulsing in mode-locked laser cavities. J Opt Soc Am B 2010; 27:2068–77.
[111] Fu X, Kutz JN. High-energy mode-locked fiber lasers using multiple transmission filters and a genetic algorithm. Opt Express 2013; 21:6526–37.
[112] Li F, Wai PKA. Energy enhancement in mode-locked fiber lasers by using multiple nonlinear optical fiber loop mirrors. Chin Opt Lett 2014; 12:S21407.
[113] Boscolo S, Turitsyn SK, Finot C. Amplifier similariton fiber laser with nonlinear spectral compression. Opt Lett 2012; 37:4531–3.
[114] Planas SA, Mansur NLP, Cruz CHB, Fragnito HL. Spectral narrowing in the propagation of chirped pulses in single-mode fibers. Opt Lett 1993; 18:699–701.
[115] Liang R, Zhou X, Zhang Z, Qin Z, Li H, Liu Y. Numerical investigation on spectral compression of femtosecond soliton in a dispersion-increasing fiber. Opt Fiber Technol 2009; 15:438–41.

[116] Chuang H-P, Huang C-B. Wavelength-tunable spectral compression in a dispersion-increasing fiber. Opt Lett 2011; 36:2848–50.
[117] Andresen ER, Thřgersen J, Keiding SR. Spectral compression of femtosecond pulses in photonic crystal fibers. Opt Lett 2005; 30:2025–7.
[118] Li M, Li Q, Spectral compression of chirped Gaussian pulse in nonlinear optical fibers with exponentially increasing dispersion, in Nonlinear Optics, 2015, p. NW4A.20.
[119] Li F, Li Q, Yuan J, Wai PKA. Highly coherent supercontinuum generation with picosecond pulses by using self-similar compression. Opt Express 2014; 22:27339–54.
[120] Diddams SA, Jones DJ, Ye J, et al. Direct link between microwave and optical frequencies with a 300 THz femtosecond laser comb. Phys Rev Lett 2000; 84:5102–5.
[121] Alfano RR, Shapiro SL. Emission in the region 4000 to 7000 Ĺ via four-photon coupling in glass. Phys Rev Lett 1970; 24:584–7.
[122] Beaud P, Hodel W, Zysset B, Weber H. Ultrashort pulse propagation, pulse breakup, and fundamental soliton formation in a single-mode optical fiber. IEEE J Quantum Electron 1987; 23:1938–46.
[123] Islam MN, Sucha G, Bar-Joseph I, Wegener M, Gordon JP, Chemla DS. Femtosecond distributed soliton spectrum in fibers. J Opt Soc Am B 1989; 6:1149–58.
[124] Islam MN, Sucha G, Bar-Joseph I, Wegener M, Gordon JP, Chemla DS. Broad bandwidths from frequency-shifting solitons in fibers. Opt Lett 1989; 14:370–2.
[125] Ranka JK, Windeler RS, Stentz AJ. Visible continuum generation in air-silica microstructure optical fibers with anomalous dispersion at 800 nm. Opt Lett 2000; 25:25–7.
[126] Graydon O. Nonlinear optics: Supercontinuum on a chip. Nat Photon 2014; 8:266.
[127] Lau RKW, Lamont MRE, Griffith AG, Okawachi Y, Lipson M, Gaeta AL. Octave-spanning mid-infrared supercontinuum generation in silicon nanowaveguides. Opt Lett 2014; 39:4518–21.
[128] Singh N, Hudson DD, Eggleton BJ. Silicon-on-sapphire pillar waveguides for Mid-IR supercontinuum generation. Opt Express 2015; 23:17345–54.
[129] Oh DY, Sell D, Lee H, Yang KY, Diddams SA, Vahala KJ. Supercontinuum generation in an on-chip silica waveguide. Opt Lett 2014; 39:1046–8.
[130] Biancalana F, Skryabin DV, Russell PSJ. Four-wave mixing instabilities in photonic-crystal and tapered fibers. Phys Rev E 2003; 68:046603.
[131] Dudley JM, Genty G, Eggleton BJ. Harnessing and control of optical rogue waves in supercontinuum generation. Opt Express 2008; 16:3644–51.
[132] Frosz MH. Validation of input-noise model for simulations of supercontinuum generation and rogue waves. Opt Express 2010; 18:14778–87.
[133] Mussot A, Lantz E, Maillotte H, Sylvestre T, Finot C, Pitois S. Spectral broadening of a partially coherent CW laser beam in single-mode optical fibers. Opt Express 2004; 12:2838–43.
[134] Lin C, Stolen RH. New nanosecond continuum for excited-state spectroscopy. Appl Phys Lett 1976; 28:216.
[135] Alfano RR. The supercontinuum laser source, 2006.
[136] Stolen RH, Lee C, Jain RK. Development of the stimulated Raman spectrum in single-mode silica fibers. J Opt Soc Am B 1984; 1:652–7.
[137] Baldeck P, Alfano R. Intensity effects on the stimulated four photon spectra generated by picosecond pulses in optical fibers. J Lightwave Technol 1987; 5:1712–5.
[138] Ilev I, Kumagai H, Toyoda K, Koprinkov I. Highly efficient wideband continuum generation in a single-mode optical fiber by powerful broadband laser pumping. Applied optics 1996; 35:2548–53.
[139] Heidt AM. Pulse preserving flat-top supercontinuum generation in all-normal dispersion photonic crystal fibers. J Opt Soc Am B 2010; 27:550–9.
[140] Hooper LE, Mosley PJ, Muir AC, Wadsworth WJ, Knight JC. Coherent supercontinuum generation in photonic crystal fiber with all-normal group velocity dispersion. Opt Express 2011; 19:4902–7.
[141] Heidt AM, Hartung A, Bosman GW, et al. Coherent octave spanning near-infrared and visible supercontinuum generation in all-normal dispersion photonic crystal fibers. Opt Express 2011; 19:3775–87.
[142] Heidt AM, Rothhardt J, Hartung A, et al. High quality sub-two cycle pulses from compression of supercontinuum generated in all-normal dispersion photonic crystal fiber. Opt Express 2011; 19:13873–9.
[143] Al-Kadry A, Li L, Amraoui ME, North T, Messaddeq Y, Rochette M. Broadband supercontinuum generation in all-normal dispersion chalcogenide microwires. Opt Lett 2015; 40:4687–90.
[144] Saitoh K, Koshiba M. Highly nonlinear dispersion-flattened photonic crystal fibers for supercontinuum generation in a telecommunication window. Opt Express 2004; 12:2027–32.
[145] Tse MLV, Horak P, Poletti F, et al. Supercontinuum generation at 1.06 μm in holey fibers with dispersion flattened profiles. Opt Express 2006; 14:4445–51.
[146] Dudley JM, Coen S. Coherence properties of supercontinuum spectra generated in photonic crystal and tapered optical fibers. Opt Lett 2002; 27:1180–2.
[147] Solli DR, Ropers C, Jalali B. Active control of rogue waves for stimulated supercontinuum generation. Phys Rev Lett 2008; 101:233902.
[148] Cheung KKY, Zhang C, Zhou Y, Wong KKY, Tsia KK. Manipulating supercontinuum generation by minute continuous wave. Opt Lett 2011; 36:160–2.
[149] Li Q, Li F, Wong KKY, Lau APT, Tsia KK, Wai PKA. Investigating the influence of a weak continuous-wave-trigger on picosecond supercontinuum generation. Opt Express 2011; 19:13757–69.
[150] Sørensen ST, Larsen C, Møller U, Moselund PM, Thomsen CL, Bang O. Influence of pump power and modulation instability gain spectrum on seeded supercontinuum and rogue wave generation. J Opt Soc Am B 2012; 29:2875–85.
[151] Lu F, Knox WH. Low noise wavelength conversion of femtosecond pulses with dispersion micro-managed holey fibers. Opt Express 2005; 13:8172–8.
[152] Vanvincq O, Barviau B, Mussot A, Bouwmans G, Quiquempois Y, Kudlinski A. Significant reduction of power fluctuations at the long-wavelength edge of a supercontinuum generated in solid-core photonic bandgap fibers. Opt Express 2010; 18:24352–60.
[153] Eggleton BJ, Luther-Davies B, Richardson K. Chalcogenide photonics. Nat Photon 2011; 5:141–8.
[154] Luther-Davies B. Flexible chalcogenide photonics. Nat Photon 2014; 8:591–3.
[155] Martínez A, Blasco J, Sanchis P, et al. Ultrafast all-optical switching in a silicon-nanocrystal-based silicon slot waveguide at telecom wavelengths. Nano Lett 2010; 10:1506–11.

[156] Zhang L, Agarwal AM, Kimerling LC, Michel J. Nonlinear Group IV photonics based on silicon and germanium: from near-infrared to mid-infrared. Nanophotonics 2013; 3:247–68.
[157] Kang Z, Yuan J, Zhang X, et al. CMOS-compatible 2-bit optical spectral quantization scheme using a silicon-nanocrystal-based horizontal slot waveguide. Sci Rep 2014; 4:7177.
[158] Koos C, Vorreau P, Vallaitis T, et al. All-optical high-speed signal processing with silicon–organic hybrid slot waveguides. Nat Photon 2009; 3:216–9.
[159] Yin L, Lin Q, Agrawal GP. Soliton fission and supercontinuum generation in silicon waveguides. Opt Lett 2007; 32:391–3.
[160] Yin L, Agrawal GP. Impact of two-photon absorption on self-phase modulation in silicon waveguides. Opt Lett 2007; 32:2031–3.
[161] Bristow AD, Rotenberg N, van Driel HM. Two-photon absorption and Kerr coefficients of silicon for 850–2200 nm. Appl Phys Lett 2007; 90:191104.
[162] Lin Q, Painter OJ, Agrawal GP. Nonlinear optical phenomena in silicon waveguides: modeling and applications. Opt Express 2007; 15:16604–44.
[163] Pearl S, Rotenberg N, van Driel HM. Three photon absorption in silicon for 2300–3300 nm. Appl Phys Lett 2008; 93:131102.
[164] Gai X, Yu Y, Kuyken B, et al. Nonlinear absorption and refraction in crystalline silicon in the mid-infrared. Laser Photon Rev 2013; 7:1054–64.
[165] Kuyken B, Ideguchi T, Holzner S, et al. An octave-spanning mid-infrared frequency comb generated in a silicon nanophotonic wire waveguide. Nat Commun 2015; 6:6310.
[166] Kippenberg TJ, Spillane SM, Vahala KJ. Kerr-nonlinearity optical parametric oscillation in an ultrahigh-Q toroid microcavity. Phys Rev Lett 2004; 93:083904.
[167] Foster MA, Levy JS, Kuzucu O, Saha K, Lipson M, Gaeta AL. Silicon-based monolithic optical frequency comb source. Opt Express 2011; 19:14233.
[168] Moss DJ, Morandotti R, Gaeta AL, Lipson M. New CMOS-compatible platforms based on silicon nitride and Hydex for nonlinear optics. Nat Photon 2013; 7:597–607.
[169] Zhang L, Mu J, Singh V, Agarwal AM, Kimerling LC, Michel J. Intra-cavity dispersion of microresonators and its engineering for octave-spanning Kerr frequency comb generation. IEEE J Sel Topics Quantum Electron 2014; 20:5900207.
[170] Griffith AG, Lau RKW, Cardenas J, et al. Silicon-chip mid-infrared frequency comb generation. Nat commun 2015; 6:6299.
[171] Del'Haye P, Coillet A, Loh W, Beha K, Papp SB, Diddams SA. Phase steps and resonator detuning measurements in microresonator frequency combs. Nat commun 2015; 6:5668.
[172] Del'Haye P, Herr T, Gavartin E, Gorodetsky ML, Holzwarth R, Kippenberg TJ. Octave spanning tunable frequency comb from a microresonator. Phys Rev Lett 2011; 107:063901.
[173] Herr T, Hartinger K, Riemensberger J, et al. Universal formation dynamics and noise of Kerr-frequency combs in microresonators. Nat Photon 2012; 6:480–7.
[174] Wang CY, Herr T, Del'Haye P, et al. Mid-infrared optical frequency combs at 2.5 μm based on crystalline microresonators. Nat commun 2013; 4:1345.
[175] Pfeifle J, Coillet A, Henriet R, et al. Optimally coherent Kerr combs generated with crystalline whispering gallery mode resonators for ultrahigh capacity fiber communications. Phys Rev Lett 2015; 114:093902.
[176] Ruehl A, Martin MJ, Cossel KC, et al. Ultrabroadband coherent supercontinuum frequency comb. Phys Rev A 2011; 84:011806(R).
[177] Kippenberg TJ, Holzwarth R, Diddams SA. Microresonator-based optical frequency combs. Science 2011; 332:555–60.
[178] Lamont MRE, Okawachi Y, Gaeta AL. Route to stabilized ultrabroadband microresonator-based frequency combs. Opt Lett 2013; 38:3478–81.
[179] Coen S, Haelterman M. Modulational instability induced by cavity boundary conditions in a normally dispersive optical fiber. Phys Rev Lett 1997; 79:4139–42.
[180] Matsko AB, Savchenkov AA, Maleki L. Normal group-velocity dispersion Kerr frequency comb. Opt Lett 2012; 37:43–5.
[181] Coen S, Erkintalo M. Universal scaling laws of Kerr frequency combs. Opt Lett 2013; 38:1790–2.
[182] Erkintalo M, Coen S. Coherence properties of Kerr frequency combs. Opt Lett 2014; 39:283–6.
[183] Herr T, Brasch V, Jost JD, et al. Temporal solitons in optical microresonators. Nat Photon 2014; 8:145–52.
[184] Leo F, Coen S, Kockaert P, Gorza S-P, Emplit P, Haelterman M. Temporal cavity solitons in one-dimensional Kerr media as bits in an all-optical buffer. Nat Photon 2010; 4:471–6.
[185] Jang JK, Erkintalo M, Murdoch SG, Coen S. Ultraweak long-range interactions of solitons observed over astronomical distances. Nat Photon 2013; 7:657–63.
[186] Herr T, Brasch V, Jost JD, et al. Mode spectrum and temporal soliton formation in optical microresonators. Phys Rev Lett 2014; 113:123901.
[187] Jang JK, Erkintalo M, Coen S, Murdoch SG. Temporal tweezing of light through the trapping and manipulation of temporal cavity solitons. Nat Commun 2015; 6:1–7.
[188] Jang JK, Erkintalo M, Luo K, Oppo G-L, Coen S, Murdoch SG. Controlled merging and annihilation of localized dissipative structures in an AC-driven damped nonlinear Schrödinger system. 2015:5.
[189] Luo K, Xu Y, Erkintalo M, Murdoch SG. Resonant radiation in synchronously pumped passive Kerr cavities. Opt Lett 2015; 40:427–30.
[190] Haelterman M, Trillo S, Wabnitz S. Dissipative modulation instability in a nonlinear dispersive ring cavity. Opt Commun 1992; 91:401–7.
[191] Coen S, Randle HG, Sylvestre T, Erkintalo M. Modeling of octave-spanning Kerr frequency combs using a generalized mean-field Lugiato-Lefever model. Opt Lett 2013; 38:37–9.
[192] Lugiato L, Lefever R. Spatial dissipative structures in passive optical systems. Phys Rev Lett 1987; 58:2209–11.
[193] Matsko AB, Savchenkov AA, Liang W, Ilchenko VS, Seidel D, Maleki L. Mode-locked Kerr frequency combs. Opt Lett 2011; 36:2845–7.
[194] Zhang L, Bao C, Singh V, et al. Generation of two-cycle pulses and octave-spanning frequency combs in a dispersion-flattened micro-resonator. Opt Lett 2013; 38:5122–5.
[195] Chembo YK, Menyuk CR. Spatiotemporal Lugiato-Lefever formalism for Kerr-comb generation in whispering-gallery-mode resonators. Phys Rev A 2013; 87:1–4.
[196] Hansson T, Modotto D, Wabnitz S. Mid-infrared soliton and Raman frequency comb generation in silicon microrings. Opt Lett 2014; 39:6747–50.
[197] Lau RKW, Lamont MRE, Okawachi Y, Gaeta AL. Effects of multiphoton absorption on parametric comb generation in silicon mi-

croresonators. Opt Lett 2015; 40:2778–81.
[198] Bao C, Zhang L, Kimerling LC, Michel J, Yang C. Soliton breathing induced by stimulated Raman scattering and self-steepening in octave-spanning Kerr frequency comb generation. Opt Express 2015; 23:18665–70.
[199] Chembo YK, Yu N. Modal expansion approach to optical-frequency-comb generation with monolithic whispering-gallery-mode resonators. Phys Rev A 2010; 82:033801.
[200] Chembo YK, Strekalov DV, Yu N. Spectrum and dynamics of optical frequency combs generated with monolithic whispering gallery mode resonators. Phys Rev Lett 2010; 104:103902.
[201] Matsko AB, Liang W, Savchenkov AA, Maleki L. Chaotic dynamics of frequency combs generated with continuously pumped nonlinear microresonators. Opt Lett 2013; 38:525–7.
[202] Hansson T, Modotto D, Wabnitz S. On the numerical simulation of Kerr frequency combs using coupled mode equations. Opt Commun 2014; 312:134–6.
[203] Peregrine D. Water waves, nonlinear Schrödinger equations and their solutions. J Austral Math Soc Ser B 1983; 25:16–43.
[204] Coste C. Nonlinear Schrödinger equation and superfluid hydrodynamics. The European Physical Journal B 1998; 1:245–53.
[205] Carretero-González R, Frantzeskakis DJ, Kevrekidis PG. Nonlinear waves in Bose–Einstein condensates: physical relevance and mathematical techniques. Nonlinearity 2008; 21:R139–R202.
[206] Bao W. The nonlinear Schrödinger equation and applications in Bose-Einstein condensation and plasma physics. Dynamics in models of coarsening, coagulation, condensation and quantization. National University of Singapore, 2007, 141.